Journal of Medicinal Chemistry

pubs.acs.org/jmc

Article

Photocaged DNA-Binding Photosensitizer Enables Photocontrol of Nuclear Entry for Dual-Targeted Photodynamic Therapy

Elyse M. Digby, Seylan Ayan, Pradeep Shrestha, Elizabeth J. Gehrmann, Arthur H. Winter, and Andrew A. Beharry*

Cite This: J. Med. Chem. 2022, 65, 16679−16694

Read Online

ACCESS | Metrics & More | Article Recommendations | Supporting Information

ABSTRACT: Photodynamic therapy (PDT) is a clinically approved cancer treatment that requires a photosensitizer (PS), light, and molecular oxygen—a combination which produces reactive oxygen species (ROS) that can induce cancer cell death. To enhance the efficacy of PDT, dual-targeted strategies have been explored where two photosensitizers are administered and localize to different subcellular organelles. To date, a single small-molecule conjugate for dual-targeted PDT with light-controlled nuclear localization has not been achieved. We designed a probe composed of a DNA-binding PS (Br-DAPI) and a photosensitizing photocage (WinterGreen). Illumination with 480 nm light removes WinterGreen from the conjugate and produces singlet oxygen mainly in the cytosol, while Br-DAPI localizes to nuclei, binds DNA, and produces ROS using one- or two-photon illumination. We observe synergistic photocytotoxicity in MCF7 breast cancer cells, and a reduction in size of three-dimensional (3D) tumor spheroids, demonstrating that nuclear/cytosolic photosensitization using a single agent can enhance PDT efficacy.

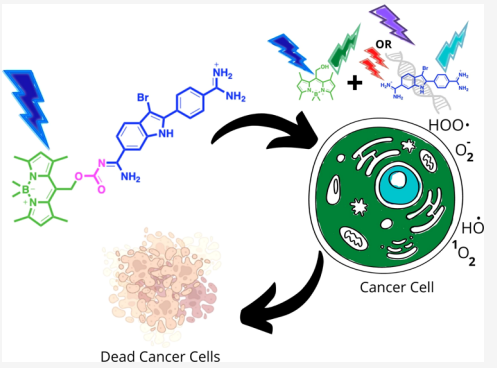

INTRODUCTION

Photodynamic therapy (PDT) is a clinically approved cancer treatment that uses the combination of a photosensitizer (PS), wavelength-specific light, and molecular oxygen to produce reactive oxygen species (ROS) that can induce cytotoxicity.[1] The process by which ROS are produced requires the PS to enter an excited singlet state, followed by intersystem crossing to an excited triplet state.[2] From here, photosensitization can occur via type I or type II mechanisms involving electron transfer to nearby oxygen-containing species or direct energy transfer to molecular oxygen, respectively.[3] Type I photosensitization produces high-energy radicals, while a Type II mechanism produces singlet oxygen, where both types of ROS can have cytotoxic effects. Since the lifetime of most ROS are on a time scale of microseconds,[4] a maximal diffusion distance corresponds to micrometers from the site of their generation.[1,4] Thus, PSs which accumulate in critical organelles (e.g., mitochondria, lysosomes[3,5,6]) and/or bind key biomolecules (e.g., DNA[1,7−10]) that are vital for maintaining cell function can cause ROS-induced damage that leads to higher photocytotoxicity.[6,11,12]

Although not yet clinically approved, several dual-targeted PDT approaches have been reported, whereby PSs localized into different organelles have led to synergetic effects with a cumulative potency that is higher than the theoretical additive effect from each PS. An early example used both hypericin and 5-aminolevulinic acid to induce HEC-1A endometrial cancer cell death.[13] Since then, other examples have included dual targeting of the lysosomes and Golgi apparatus,[14] lysosomes and mitochondria,[15] mitochondria and plasma membrane,[16] and plasma membrane and nuclei.[7,17] Although effective cell death has been observed in these studies, some drawbacks include no well-defined cell localization of the PSs making it difficult to deduce the effectiveness of targeting a given organelle[14] and the requirement to administer two separate PSs poses pharmacodynamic challenges *in vivo*.[13,14] Alternatively, the Zhang group constructed single PS agent nanovesicles to target the plasma membrane followed by mitochondria or nuclei by incorporating chimeric peptides as targeting motifs.[16,17] Although effective,[18] generally the administration of PSs (or drugs) as nanoparticles has challenges including systemic toxicity and variation in physiochemical properties during large-scale manufacturing.[19] To this regard, small-molecule dual-targeted PDT strategies have been advantageous, though many use PSs that contain metals such as platinum[20] or iridium,[21,22] which make them more susceptible to off-target effects by complexing with biological milieu[23] and may contribute to dark toxicity.[24] A single small-molecule PS agent capable of inducing oxidative

Received: September 13, 2022
Published: December 8, 2022

https://doi.org/10.1021/acs.jmedchem.2c01504
J. Med. Chem. 2022, 65, 16679−16694

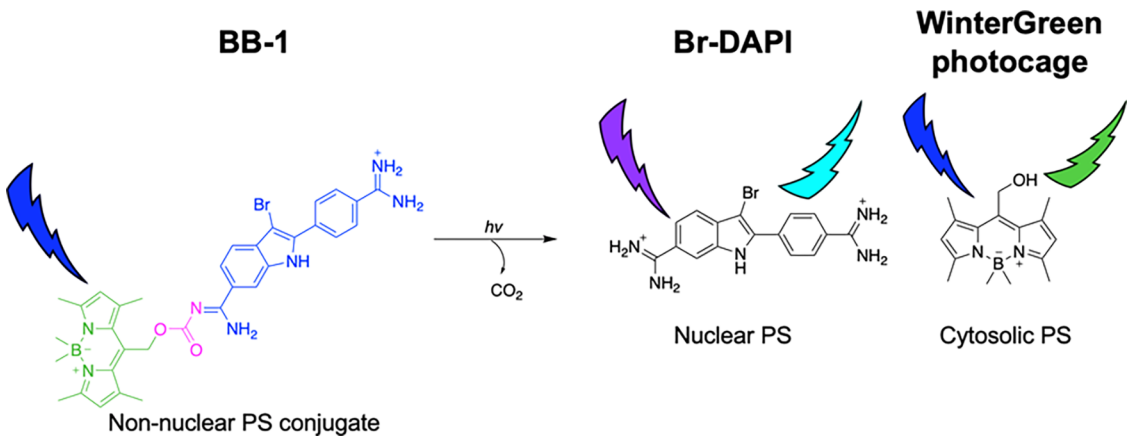

Figure 1. Proposed mechanism of **BB-1** uncaged via illumination with blue light to release free Br-DAPI and WinterGreen. Free WinterGreen produces singlet oxygen during uncaging illumination, while free Br-DAPI localizes to nuclei, binds DNA, and produces ROS upon illumination. Br-DAPI = blue, WinterGreen photocage = green, carbamate linker = pink.

damage in two distinct cell organelles with defined localization that does not consist of potentially cytotoxic materials such as metals has not yet been reported. Thus, it would be beneficial to develop such an agent to explore its efficacy for dual-targeted PDT.

Given the vital role of the nucleus for cancer cell survival, DNA-targeted anticancer treatment (compared to enzyme-targeted anticancer therapies) is a promising strategy to increase therapeutic efficacy,[7,21,25] as multiple cancers can be targeted simultaneously, including those that have metastasized.[26,27] DNA-targeted dual PSs in particular have the advantage of being more effective relative to traditional PSs when treating multidrug-resistant cancers since the effective concentration of PS is higher (i.e., less PS pumped out via efflux pumps) so that therapeutic effects can be amplified.[7] Despite DNA damage constituting the most critical inducer of apoptosis,[3,28,29] making it one of the primary targets for anticancer drugs,[26,27] the nucleus has been generally under-targeted for dual-targeted PDT. However, the few reports on targeting the nucleus for dual-targeted PDT have been successful.[7,17,20,21] For example, in a recent study, a functionalized iridium complex was designed to target mitochondria and then nuclei.[21] Tian *et al.* also reported iridium-based complexes that target the nucleus and then migrate sequentially to mitochondria.[22] Zhou *et al.* recently proposed a strategy involving cationic triphenylamine PSs, which they report to bind DNA and potentially target mitochondria.[25] However, in all cases, although effective cell death with high potency was observed, with even damage to DNA demonstrated in some cases (i.e., via gel electrophoresis[21] or immunofluorescence staining[7]), these studies had inefficient targeting of the nucleus, required carriers to deliver the PSs to the nucleus, administrated two PSs separately, or included metal complexes in their design.

In this report, we describe a single small-molecule PS conjugate made up of two different PSs, whereby upon illumination, the individual PSs are released. Given the promising studies in dual-targeted PDT involving nuclear targeting, we employed our recently developed DNA-binding PS, Br-DAPI,[9] where efficient localization in the nucleus is observed only upon photo-cleavage, while the photocage-PS WinterGreen remains mostly in the cytosol.

RESULTS AND DISCUSSION

Description of Dual-Targeting PDT Strategy Using a Photocage-PS Conjugate. We previously reported a brominated 4′,6-diamidino-2-phenylindole (DAPI) derivative, Br-DAPI, as a DNA-binding PS able to induce double-strand DNA breaks upon illumination and cause dose-dependent photocytotoxicity in both cancer cells and bacteria.[9,30] Br-DAPI also increases its fluorescence once bound to DNA in nuclei of mammalian cells and in bacteria, providing a method for detecting its subcellular accumulation and thus, determining the optimal time to illuminate.[9] Moreover, we showed that Br-DAPI is 2-photon (2P) active where PDT in bacteria using a 2P laser caused bacterial cell death.[30] However, despite its promise for photodynamic cancer therapy, Br-DAPI's full potential as a light-activated DNA damaging agent was limited by its poor cell permeability. Br-DAPI contains two aryl amidines, each carrying a 1+ charge (overall 2+ charge state) at physiological pH, making the molecule very polar. We reasoned that modification of an amidine with a large hydrophobic moiety would increase the overall hydrophobicity, and if the moiety was linked via a carbamate, the amidine pK_a would be lowered (as observed in other aryl amidine compounds[31]), thereby reducing the overall charge state to 1+, leading to an increase in cell permeability and subsequent potency. Moreover, since Br-DAPI is a DNA-binding/intercalating agent, although not observed in cell culture studies, it is likely that unwanted dark toxicity in healthy cells *in vivo* would occur. Thus, it would be beneficial to prevent nuclear entry of Br-DAPI under dark conditions and control DNA-binding spatially using light.

To improve Br-DAPI for PDT and explore the possibility of a single molecule capable of dual-targeted PDT with a DNA-targeted PS, we sought to modify Br-DAPI's amidine with another PS. To achieve differential cellular localization, we require the ligated PSs to separate to release Br-DAPI when inside a cell. Winter and colleagues reported photocaged cathepsin B inhibitors, where activation of the inhibitors occurred after illumination with visible light to induce photocleavage of a BODIPY-based photocage called WinterGreen.[32] Interestingly, WinterGreen photocage, once uncaged, produces singlet oxygen.[32] We hypothesized that modification of Br-DAPI with WinterGreen would result in ROS production from the WinterGreen photocage during the uncaging illumination

https://doi.org/10.1021/acs.jmedchem.2c01504
J. Med. Chem. 2022, 65, 16679−16694

Scheme 1. Synthesis of BB Probes Using 4-Nitrophenyl Carbonate WinterGreen and Br-DAPI[a]

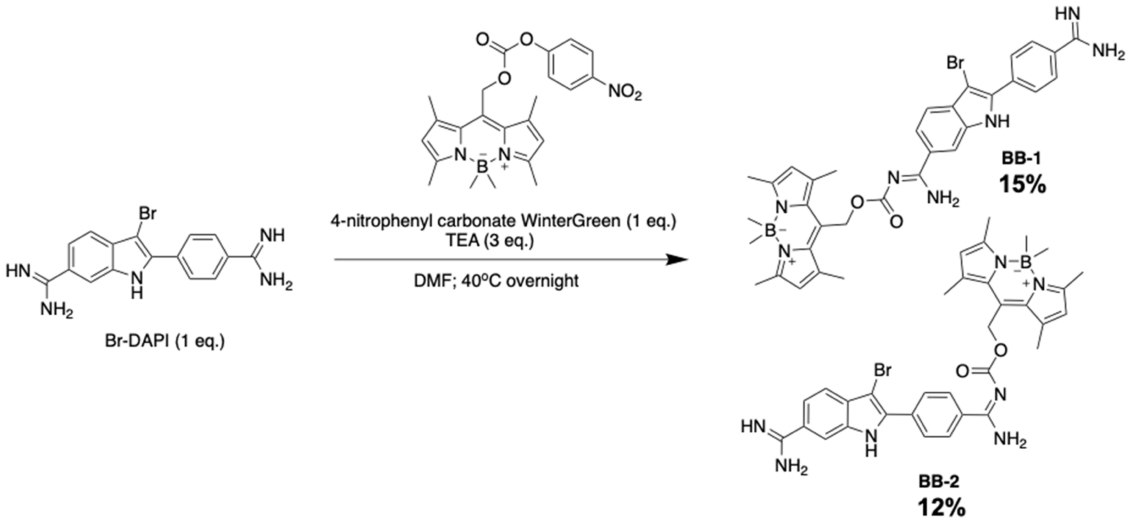

[a]Nucleophilic substitution yielded **BB-1** whereby the photocage is attached to the phenylindole amidine, and **BB-2** whereby the photocage is attached to the phenyl amidine.

period, followed by ROS production in the nucleus once Br-DAPI was released and illuminated. Figure 1 shows the predicted activation mechanism of the Br-DAPI-WinterGreen conjugate (i.e., **BB-1**), upon illumination with the appropriate wavelength of light. Molecules capable of nuclear entry are often characterized by having a high positive charge and a lower molecular weight so that movement through nuclear pore complexes via passive diffusion is more probable.[33,34] Thus, we expected that modification of one of the amidines on Br-DAPI should alter the cellular location of the resulting conjugate to a site other than the nucleus.

Synthesis of Dual-Targeted PDT Probe. Both Br-DAPI and WinterGreen were synthesized using previously reported procedures (Scheme S1).[9,35,36] To synthesize **BB**, the alcohol of the WinterGreen photocage was first activated with 4-nitrophenyl chloroformate (Scheme S2), followed by nucleophilic substitution by the amidines on Br-DAPI (Scheme 1), to yield a final conjugate linked via a carbamate linkage. Under these reaction conditions, the WinterGreen photocage is attached to either the phenylindole amidine (**BB-1**) or the phenyl amidine (**BB-2**) which were separable using reverse-phase high-performance liquid chromatography (RP-HPLC) (Scheme 1). All intermediates and final probes were purified using silica chromatography and/or RP-HPLC and characterized using NMR and high-resolution mass spectrometry (HRMS) (see Supporting Information).

Prediction of Compound Permeability *In Cellulo*. To predict whether the addition of WinterGreen via a carbamate linkage would increase the cellular permeability of Br-DAPI, we measured the $-\text{Log}\,P_e$ value (i.e., effective permeability) using a parallel artificial membrane permeability assay (PAMPA). Previous reports on an amidine-based prodrug masked by a carbamate linkage measured the formal charge of the amidine at pH 7.4 to be reduced from 1+ to 0, where the pK_a of the nitrogen dropped from 12.4 to 6.7.[31] The $-\text{Log}\,P_e$ of Br-DAPI was measured to be 7.04 ± 0.01, while **BB-1** and **BB-2** were 5.90 ± 0.01 and 5.69 ± 0.01, respectively (Figure S1). Based on experimental data for commonly used drugs, $-\text{Log}\,P_e$ values <6 are considered to have good membrane permeability via passive diffusion.[37] Thus, the experimentally measured values for Br-DAPI and its corresponding **BB** conjugates suggest that the effective concentration of Br-DAPI *in cellulo* after uncaging will be higher compared to cells treated with Br-DAPI alone.

Effect of Photo-Caging on the Photophysical Properties of Br-DAPI. To evaluate the effect on the photophysical properties of conjugating Br-DAPI with WinterGreen photocage, we compared the photophysical properties of the **BB** probes with free Br-DAPI and WinterGreen. **BB-1** had maximum absorbance at 340 nm and at 525 nm and **BB-2** at 350 and 520 nm (Figure S2), with **BB-2** slightly red-shifted from free Br-DAPI (λ_{max} 340 nm) and both probes red-shifted from WinterGreen (λ_{max} 505 nm). Interestingly, the fluorescence of the Br-DAPI moiety (λ_{ex} 345 nm) in **BB-1** and **BB-2** was quenched by a factor of 4 compared to free Br-DAPI (Figure S3; when comparing fluorescence for each compound at $\lambda_{em,max}$ = 450 nm either in the presence or absence of calf thymus DNA (CT-DNA)). As we did not observe emission from WinterGreen upon Br-DAPI excitation at 345 nm (which would be expected if FRET was occurring), we hypothesized that the quenching may be due to photo-induced electron transfer. To probe for which part of the modification to Br-DAPI dictates the quenching mechanism (i.e., the carbamate linkage or WinterGreen), we synthesized Br-DAPI containing a methyl carbamate on the phenylindole amidine (Scheme S3), which lacks WinterGreen. Br-DAPI methyl carbamate had the same maximum absorbance (340 nm) as Br-DAPI and similar fluorescence intensities (Figure S4), with only ∼1.6-fold quenching compared to native Br-DAPI. Hence, the minimal changes in the fluorescence intensity suggests that WinterGreen is primarily responsible for the quenching effect observed when Br-DAPI is in the form of the **BB** probes.

Since Br-DAPI increases in fluorescence upon binding DNA, we also probed for changes in fluorescence from **BB-1** and **BB-2** to investigate their ability to bind DNA. To a solution containing 20 μM **BB-1** or **BB-2**, CT-DNA was added at increasing concentrations. Interestingly, despite their larger size and reduced charge state (1+ compared to 2+ for free Br-DAPI)[32,33,38] an increase in fluorescence intensity at 450 nm

https://doi.org/10.1021/acs.jmedchem.2c01504
J. Med. Chem. 2022, 65, 16679−16694

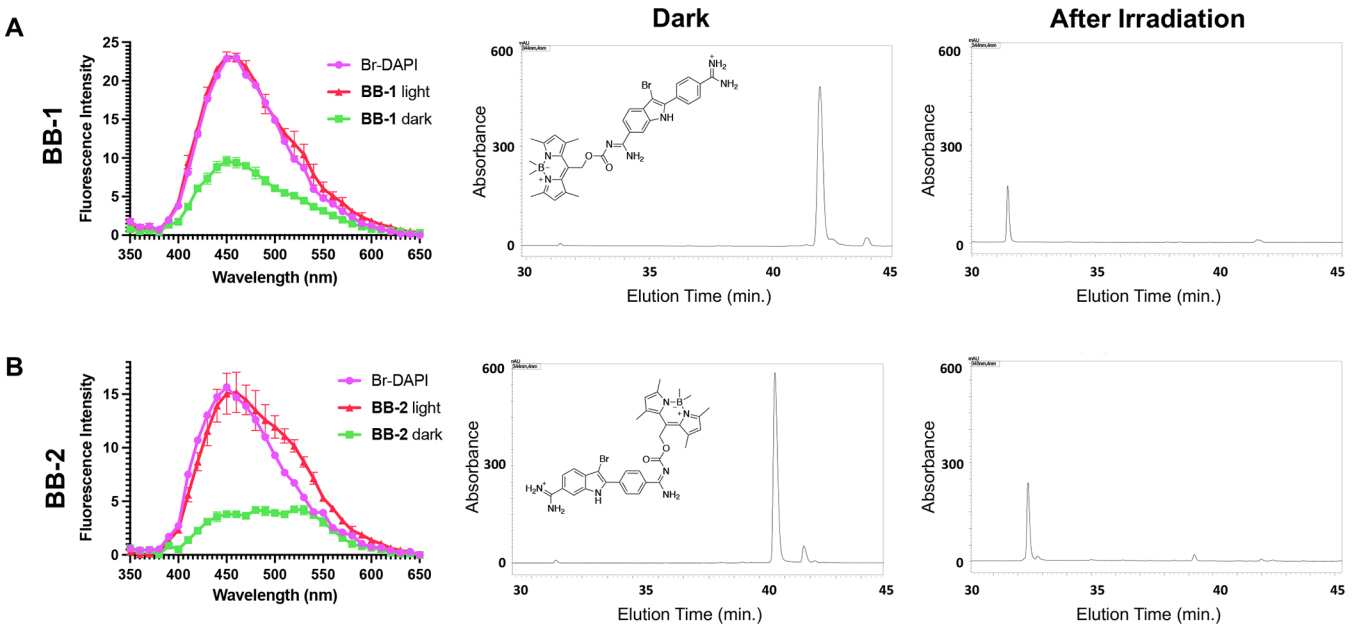

Figure 2. (A, B) Left: Br-DAPI uncaging in PBS pH 7.4 at 37 °C, monitored by fluorescence; 1 μM **BB** compounds (**BB-1** and **BB-2**) in the presence of saturating amounts of CT-DNA (60 μM) initially has low fluorescence (green). After 20 min of 480 nm illumination (3.1 J cm^{-2}), the fluorescence intensity of the **BB** samples increases (pink) to match that of 1 μM Br-DAPI (+60 μM CT-DNA) (red). Independent samples (n = 3). λ_{ex} 345 nm. Middle and right: Characterization of the photo-release products by analytical RP-HPLC. Middle: 50 μM **BB** compounds after 3 h incubation in PBS pH 7.4 at 37 °C in the dark show retention time of expected intact **BB** probes. Right: After 20 min of 480 nm illumination (3.1 J cm^{-2}) of solutions containing 50 μM **BB** compounds in PBS pH 7.4, no peak representing intact probe is observed, but a new peak appears at 32 ± 0.5 min corresponding to Br-DAPI. Absorbance monitored at 345 nm. Independent samples (n = 2).

was observed suggesting **BB** compounds still bind to CT-DNA (note the maximum fluorescence was still 4-fold lower compared to Br-DAPI in the presence of saturating amounts of CT-DNA (Figure S3), but this is consistent with the fluorescence quenching observed in the absence of DNA). The binding constants (K_D) for **BB-1** and **BB-2** to CT-DNA were ~6 and 10 μM, respectively, comparable to Br-DAPI (K_D ~19 μM). We hypothesize the stronger binding to DNA with **BB** compounds compared to free Br-DAPI is due to the planar conjugated structure of WinterGreen's BODIPY core, capable of intercalating with DNA base pairs as previously observed with BODIPY dyes modified with cationic groups.[39−41] To test for WinterGreen's interaction with CT-DNA, we monitored the primary region of WinterGreen photocage's absorption spectrum (400−700 nm) in **BB-1** (20 μM) upon titration of CT-DNA (Figure S3). A decrease as well as a redshift in its absorption spectrum was observed, which is expected for DNA-binding BODIPY compounds.[39] Overall, although **BB-1** and **BB-2** have an unexpected higher binding affinity to CT-DNA compared to Br-DAPI, we considered that the addition of WinterGreen to Br-DAPI might prevent the Br-DAPI conjugate from entering the nucleus due to its reduced charge state,[33,34] and thus once uncaged can still permit dual-targeted PDT.

Photo-Release Studies of Br-DAPI from BB Conjugates. To assess the photo-release of Br-DAPI from **BB-1** and **BB-2**, we first used fluorescence since the **BB** conjugates were found to be quenched compared to free Br-DAPI. We measured the fluorescence spectra of the **BB** probes before and after light illumination and compared them to that of Br-DAPI at the same concentration with saturating amounts of CT-DNA to maximize fluorescence intensities for better confidence in the measurements (i.e., since Br-DAPI has a low fluorescence quantum yield when it is not bound to DNA). The initial fluorescence spectra of 1 μM **BB-1** and **BB-2** in phosphate-buffered saline (PBS) pH 7.4 (containing 60 μM CT-DNA) were notably lower than that of 1 μM Br-DAPI (containing 60 μM CT-DNA). However, after 20 min of illumination using a mercury lamp (3.1 J cm^{-2}) with a 450−495 nm excitation filter (referred to herein as 480 nm illumination) the resulting emission spectra matched that of native Br-DAPI, suggesting that Br-DAPI is uncaged (Figure 2A,B, left). To further confirm photo-release and to characterize the photo-release products, we performed analytical RP-HPLC on 50 μM **BB-1** and **BB-2** and Br-DAPI after 3 h incubation in PBS pH 7.4 at 37 °C in the dark, and on 50 μM **BB-1** and **BB-2** after 20 min of 480 nm illumination (3.1 J cm^{-2}). Under dark conditions, Br-DAPI elutes at 32 min (Figure S5) while **BB-1** and **BB-2** at 42 and 40 min, respectively (Figure 2A,B, middle). The single peak on HPLC observed for **BB** probes (42 and 40 min) after 3 h incubation in the dark suggests the carbamate linkage between Br-DAPI and WinterGreen is stable toward background hydrolysis at least for the 3 h incubation period. This was further confirmed by measuring the fluorescence intensity of **BB** probes before and after 3 h incubation in the dark, where minimal increase in the fluorescence intensity indicates no Br-DAPI is being released (i.e., no spontaneous dark hydrolysis) (Figure S6). After illumination, we observed a new peak at 32 ± 0.5 min for **BB-1** and **BB-2**, corresponding to Br-DAPI, and the disappearance of the initial peaks for intact **BB** probes (Figure 2A,B, right), demonstrating the photo-release of Br-DAPI. We further confirmed the identities of the photo-uncaged products by comparing their absorption spectra to that of Br-DAPI and confirming that the mass of the new peaks are consistent with Br-DAPI (355.04 g mol^{-1}) (Figure S7). We note that no new peak for the released WinterGreen photocage was observed,

https://doi.org/10.1021/acs.jmedchem.2c01504
J. Med. Chem. 2022, 65, 16679−16694

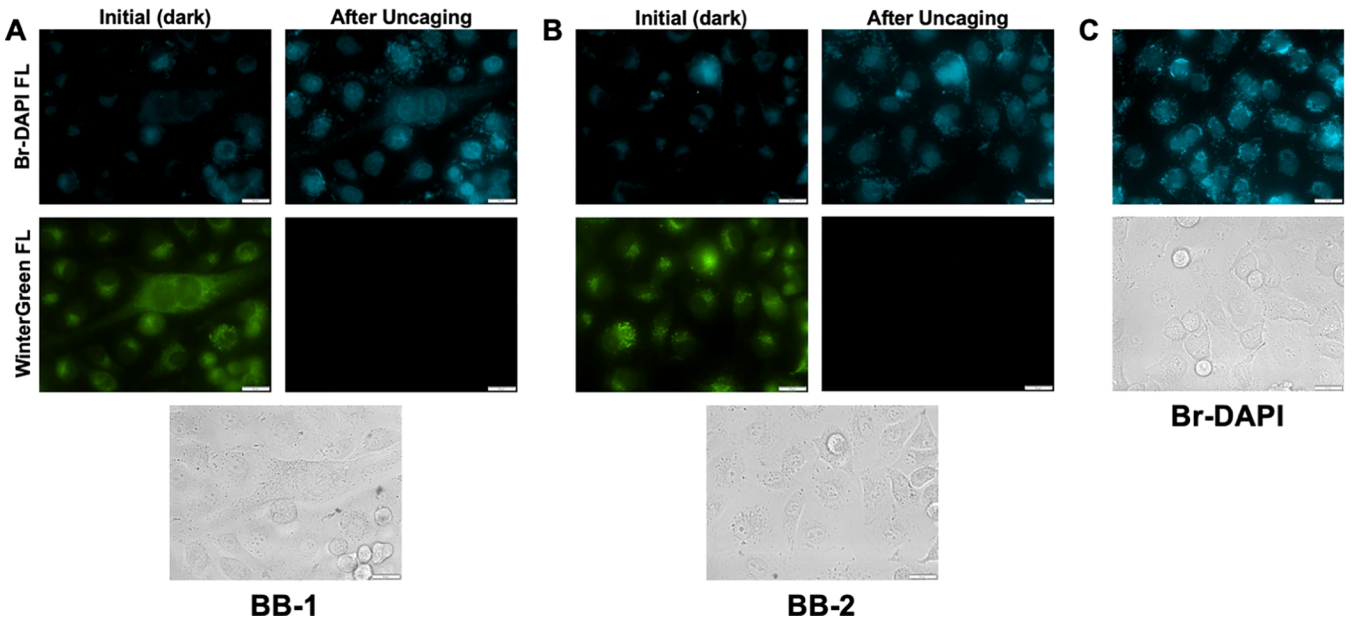

Figure 3. Photo-uncaging (A) **BB-1** and (B) **BB-2** (3 μM) in MCF7 breast cancer cells. In the dark, only green fluorescence from WinterGreen photocage was observed, while minimal cyan fluorescence and no nuclear signals were present. After 480 nm illumination (10 min, 1.6 J cm^{-2}), nuclear cyan fluorescence representing Br-DAPI release and binding to DNA was observed, while minimal green fluorescence was present. (C) Incubation of native Br-DAPI (3 μM) in MCF7 breast cancer cells demonstrate nuclear signals. Independent samples (n = 3). 40× magnification, scale bar = 20 μm. Br-DAPI imaged using a DAPI filter set (λ_{ex} 350−405 nm, λ_{em} 415−470 nm) and WinterGreen photocage using an EGFP filter set (λ_{ex} 450−495 nm, λ_{em} 500−550 nm).

since illumination during this period results in photobleaching (Figure S8).[36]

Cellular Localization of BB Probes. We next determined whether photo-release of **BB** results in differential cellular localization of the two PSs, Br-DAPI and WinterGreen. We looked for changes in the intracellular localization using the green fluorescence from the WinterGreen photocage and cyan fluorescence from Br-DAPI when bound to DNA (i.e., in the nucleus). All fluorescence observed was above background (i.e., untreated cells) for both filter sets used (i.e., DAPI and EGFP, for Br-DAPI and WinterGreen, respectively) (Figure S9). MCF7 breast cancer cells were treated with **BB-1** (3 μM) for 1 h, then washed once with PBS, and imaged. Only minimal cyan fluorescence over background was observed when exciting the Br-DAPI moiety of **BB-1** (λ_{ex} 350−405 nm, λ_{em} 415−470 nm), with no fluorescence from the nucleus (Figure 3A). We hypothesized that the few non-nuclear, cyan fluorescent signals above background could be due to nonspecific binding after the washing, which is an important step when using enhancer fluorescence DNA dyes.[42,43] When exciting WinterGreen of **BB-1** (λ_{ex} 450−495 nm, λ_{em} 500−550 nm), we observed bright green fluorescence over background in the cytosol and mitochondria (Figure S10), confirming that the intact **BB-1** probe is not present in the nucleus (Figure 3A). Upon 480 nm illumination of the MCF7 cells for 10 min (1.6 J cm^{-2}), bright cyan fluorescence signals in nuclei of the cells were observed, suggesting that Br-DAPI is released under the uncaging conditions and relocates to nuclei (Figure 3A). Moreover, the green fluorescence from WinterGreen became essentially zero, which is consistent with its photobleaching properties. Uncaging in MCF7 cells incubated with **BB-2** (3 μM) also showed the same nuclear localization upon photo-uncaging as observed with **BB-1** (Figure 3B). When comparing the photo-uncaged nuclei fluorescence of **BB-1** or **BB-2** to nuclei fluorescence from Br-DAPI at the same concentration (3 μM), similar nuclear signals for Br-DAPI were observed (Figure 3C). Photo-uncaging of **BB** probes were also tested in A549 lung cancer cells and HeLa cervical cancer cells which showed differential cellular localization similar to MCF7 cells (Figure S11).

To determine which modification to the amidine on the Br-DAPI scaffold dictates nuclear permeability (the carbamate or WinterGreen), we incubated MCF7 cells with Br-DAPI methyl carbamate (~3 μM) for 1 h, washed once with PBS, and imaged. Cyan fluorescence was clearly localized to the nuclei (Figure S12), demonstrating that nuclear permeability of Br-DAPI can be controlled by the addition of steric hindrance (e.g., WinterGreen) as opposed to a change in the charge state (i.e., 2+ to 1+). Finally, although **BB** probes showed good stability toward hydrolysis under physiological conditions in solution (Figure S6), mammalian cells contain esterases that can potentially hydrolyze carbamate linkages.[44] Cancer cells (MCF7, A549, and HeLa) were incubated with **BB-1** or **BB-2** (2 μM) for 1 h, washed once with PBS, and incubated in the dark for an additional 1 h on a heated microscope stage. No observable cyan fluorescence was in nuclei at 0 h and 2 h time points following the 1 h incubation (Figure S13) demonstrating that no Br-DAPI is released due to hydrolysis by general esterases. We further tested for hydrolytic stability of **BB-1** toward enzymatic systems within a clinical setting range (24 h), where minimal hydrolysis was observed for up to 2 μM **BB-1** (Figure S14).

Photosensitization Efficacy Monitored by ROS Production. To demonstrate the ability of **BB** probes and Br-DAPI to produce ROS in the absence of biological matrices, we used the general ROS sensor, 2′,7′-dichlorodihydrofluorescin diacetate ($DCFH_2DA$), which can be chemically deacetylated using 0.1 M $NaOH_{(aq)}$ to nonfluorescent 2′,7′-dichlorodihydrofluorescin ($DCFH_2$).[45] Samples containing 1 μM Br-DAPI, **BB-1**, or **BB-2** and 1 μM $DCFH_2$ in PBS, were

https://doi.org/10.1021/acs.jmedchem.2c01504
J. Med. Chem. 2022, 65, 16679−16694

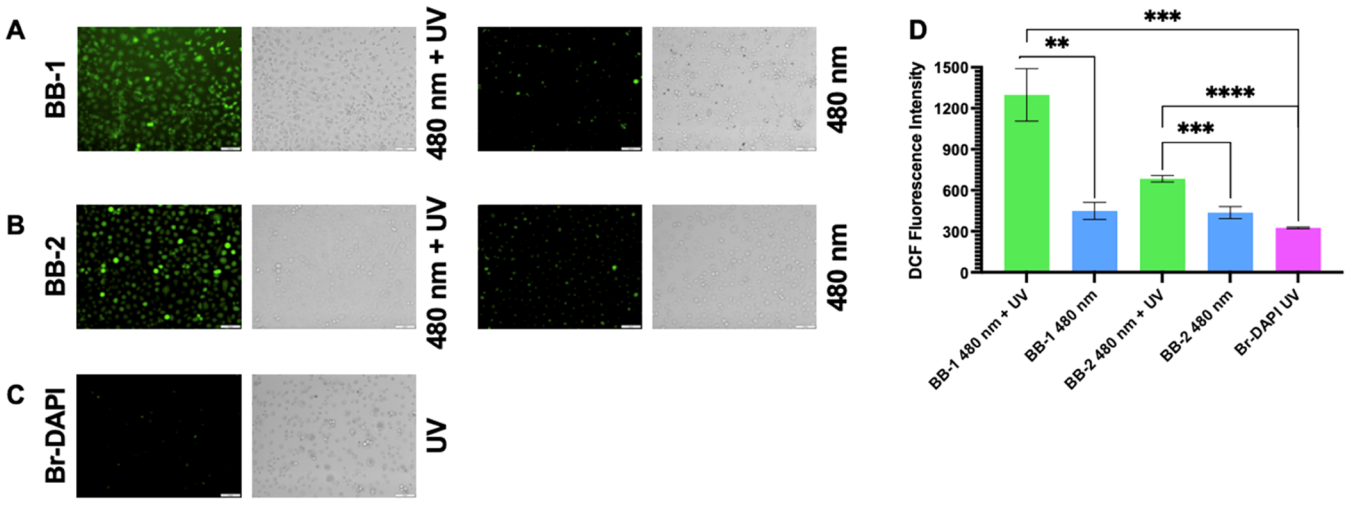

Figure 4. ROS production in MCF7 cells by (A) **BB-1** or (B) **BB-2** (2 μM) after 480 nm illumination (15 min, 2.3 J cm^{-2}) + UV (5 min, 8.0 J cm^{-2}) (left) or 480 nm illumination only (15 min, 2.3 J cm^{-2}) (right), compared to (C) Br-DAPI (2 μM) treated with UV illumination (5 min, 8.0 J cm^{-2}). ROS monitored by green fluorescence of DCF produced upon ROS-mediated oxidation of $DCFH_2$ (10 μM). (D) Quantification of the mean fluorescence intensity of DCF for each treatment shows a statistically significant difference between dual photosensitization with **BB** probes and single photosensitization with **BB** probes or Br-DAPI. Analyzed by two-tailed *t*-test, *p*-value <0.05 indicated by *. Independent samples (n = 3). 10× magnification, scale bar = 100 μm. DCF imaged using an EGFP filter set (λ_{ex} 450−495 nm, λ_{em} 500−550 nm).

illuminated with 1P or 2P light, and the fluorescence from DCF (oxidized product of the ROS sensor) was measured (Figure S15). **BB-1** showed the highest ROS production with 1P dual illumination conditions (480 nm illumination (15 min, 2.3 J cm^{-2}) + UV (5 min, 8.0 J cm^{-2})), while single-illumination with Br-DAPI was lower (UV (5 min, 8.0 J cm^{-2})). The higher ROS production was also observed when comparing **BB** probes after photo-uncaging (480 nm illumination (15 min, 2.3 J cm^{-2})) and 2P illumination with ROS produced by Br-DAPI after 2P illumination (780 nm 2P (10 s, 16 J)). The ROS-producing ability of **BB** compounds was then measured *in cellulo* using $DCFH_2DA$, which enters cells via passive diffusion where intracellular esterases cleave the acetate groups to produce $DCFH_2$.[45] MCF7 cells were incubated with **BB-1** or **BB-2** (2 μM) in the dark for 1 h, then incubated with 10 μM $DCFH_2DA$ for 30 min, with a wash after each incubation step. Treated cells were imaged for DCF fluorescence after 480 nm illumination (15 min, 2.3 J cm^{-2}) and then after additional illumination with a UV lamp (365 nm, 5 min, 8.0 J cm^{-2}). Strong DCF fluorescence was observed in cells treated with **BB** and 480 nm + UV light compared to illumination **BB** with 480 nm light alone ($p < 0.05$) (Figure 4), with minimal background signal from the ROS sensor alone in cells illuminated but with no PS (Figure S16). The production of ROS from 480 nm illumination is consistent with WinterGreen's ability to produce singlet oxygen[32] whereby once uncaged has a measured quantum yield of 0.42 ± 0.04 (Figure S17). The same experiment with **BB** probes were carried out in A549 and HeLa cells (Figure S18) that yielded different amounts of ROS under each illumination condition, which we hypothesize is due to differences among cancer cells in their response to ROS including the ability to scavenge[46] or produce secondary ROS.[47−49] We note that the effect of UV light only on the **BB** compounds, that is, Br-DAPI's ability to produce ROS in the presence of WinterGreen, could not be accurately determined since UV light causes some degree of photo-uncaging. Finally, to determine if our dual-PS, **BB**, produces more ROS than the original, single PS, Br-DAPI, we performed the same experiment above using Br-DAPI (2 μM) and UV light treated at the same dose (5 min, 8.0 J cm^{-2}) (Figure 4C). In all three cell lines, we observed less ROS production with Br-DAPI compared to our **BB** compounds, with the largest difference (~3-fold) in MCF7 cells. The lower amount of ROS production from Br-DAPI is consistent with the imaging experiments whereby Br-DAPI's ability to permeate cells is poorer compared to **BB**.

Evidence of DNA Photo-Oxidation and Double-Stranded DNA Breaks. To demonstrate that photo-uncaged Br-DAPI was able to facilitate ROS-induced oxidative DNA damage, we performed gel electrophoresis on circular, double-stranded DNA (dsDNA) (70 ng of pCMV-PARP1-3xFlag-WT) treated with 10 μM each **BB** probe and 480 nm illumination (15 min, 2.3 J cm^{-2}) + UV (5 min, 8.0 J cm^{-2}). Samples were denatured prior to loading on a 1% agarose gel containing ethidium bromide (fluorescent dye used to visualize the DNA and determine the extent of damage). Plasmid DNA untreated or under each illumination condition showed 3 bands, where the top faint band is linear, middle band is supercoiled, and the bottom band is the open circular form of plasmid DNA.[50] All illumination treatments where a PS was present resulted in the disappearance of intact plasmid DNA bands, and the appearance of a smear of unresolved bands at lower molecular weights (Figure 5). Interestingly, those treated with **BB-1** eliminated all initial intact DNA (i.e., no open circular DNA is observed in contrast to Br-DAPI and **BB-2**) and produced the smallest DNA fragments. More damage was observed with **BB-1** because photo-uncaging produces ROS due to the presence of WinterGreen which *in vitro* is in close proximity to the DNA. To confirm that dsDNA breaks are also produced in the presence of biological matrices, we employed the use of the γH2A.X assay, where γH2A.X is a histone protein that gets phosphorylated in the presence of dsDNA breaks.[51] MCF7 cells were treated with 3 μM **BB-1** or Br-DAPI, treated with 480 nm illumination (15 min, 2.3 J cm^{-2}) + UV (5 min, 8.0 J cm^{-2}) or UV (5 min, 8.0 J cm^{-2}), respectively, and left to incubate for 2 h. The cells were then fixed and incubated with a γH2A.X antibody tagged with Alexa 488, where foci within nuclei (co-stained with DAPI) are

https://doi.org/10.1021/acs.jmedchem.2c01504
J. Med. Chem. 2022, 65, 16679−16694

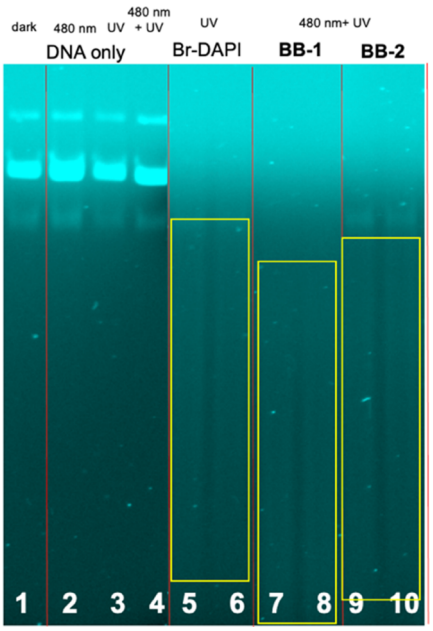

Figure 5. Br-DAPI or **BB** probes (10 μM) incubated with plasmid DNA (70 ng; pCMV-PARP1-3xFlag-WT, 7146 bp length) in PBS pH 7.4, followed by illumination with UV (5 min, 8.0 J cm^{-2}) for Br-DAPI (Lanes 5−6), or 480 nm illumination (15 min, 2.3 J cm^{-2}) + UV (5 min, 8.0 J cm^{-2}) for **BB-1** (Lanes 7−8) and **BB-2** (Lanes 9−10), respectively. Compared to plasmid DNA only (i.e., no PS), in the dark (Lane 1) and under irradiation conditions (Lane 2 = 480 nm, Lane 3 = UV, Lane 4 = 480 nm + UV), DNA treated with Br-DAPI or **BB** probes and illumination showed disappearance of intact plasmid and the presence of smears demonstrating photo-cleavage. Independent samples (n = 2).

representative of regions where dsDNA breaks are located[52] (Figure S19; γH2A.X-Alexa 488 was shown in red and DAPI in blue such that pink fluorescence for overlayed images represents dsDNA breaks in the nucleus). We observe more pink foci in nuclei for cells treated with **BB-1** compared to Br-DAPI. Since the extent of DNA damage *in vitro* by **BB-1** and Br-DAPI are similar, the higher damage of **BB-1** in cells suggests that its higher cell permeability increases the effective concentration of Br-DAPI in the nucleus, and thus oxidative damage toward DNA to be greater compared to Br-DAPI when administered in its free form. Both gel electrophoresis and the γH2A.X assay demonstrate that the Br-DAPI released after photo-uncaging **BB-1** results in oxidative damage to dsDNA.

Synergistic Photocytotoxicity from Dual Photosensitization with BB Probes. We next sought to determine whether the higher ROS production from our dual-PS, **BB** probes, results in notably higher photocytotoxicity compared to Br-DAPI. MCF7, A549, and HeLa cells were incubated for 1 h with **BB-1** (0−32 μM), **BB-2** (0−32 μM), or Br-DAPI (0−64 μM), followed by one wash with PBS. **BB** probes were treated with 480 nm light (15 min, 2.3 J cm^{-2}) followed by UV illumination (5 min, 8.0 J cm^{-2}) or 480 nm illumination (15 min, 2.3 J cm^{-2}) only, while cells incubated with Br-DAPI were treated with UV illumination (5 min, 8.0 J cm^{-2}). The cells treated with or without light (light and dark, respectively) were incubated overnight in complete growth media and then assayed for cell viability using an MTT assay 24 h post-treatment. The cells treated without light exhibited minimal dark cytotoxicity (Figures 6 and S20), while the light-treated cells produced dose−response curves (Figures 6 and S20) with CC_{50} values (the concentration that reduces the number of viable cells by 50%) calculated relative to untreated cells (i.e., no compound or light illumination) which are summarized in

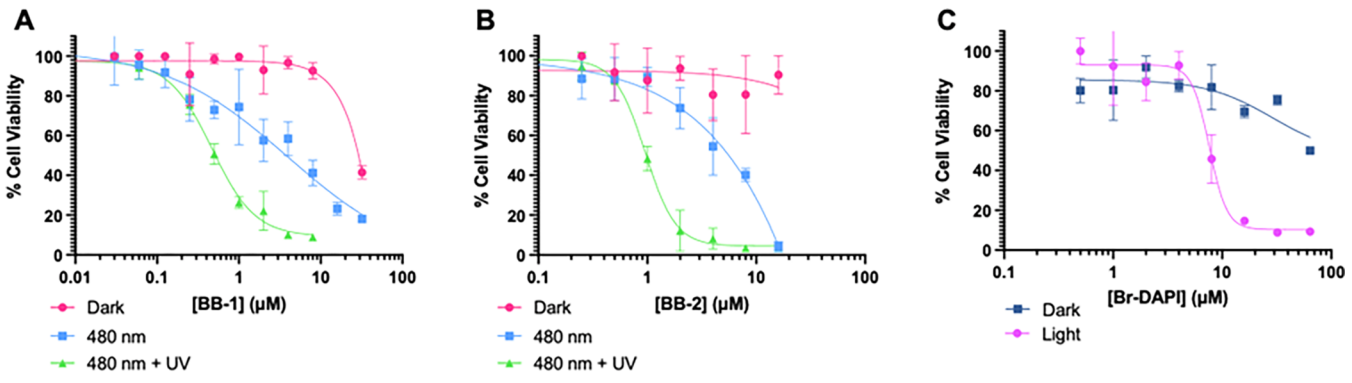

D

MCF7	CC_{50} (μM)		
Illumination Conditions	**BB-1**	**BB-2**	**Br-DAPI**
Dark	> 10	> 16	> 64
480 nm	4 ± 1	5.8 ± 0.6	n/a
480 nm + UV	0.47 ± 0.06	0.6 ± 0.03	n/a
UV	n/a	n/a	7.6 ± 0.5

Figure 6. Dose−response curves were obtained for MCF7 cells treated with (A) **BB-1**, (B) **BB-2**, or (C) Br-DAPI under dark and light conditions (**BB** probes with 480 nm illumination (15 min, 2.3 J cm^{-2}) or 480 nm illumination (15 min, 2.3 J cm^{-2}) + UV (5 min, 8.0 J cm^{-2}), Br-DAPI with UV (5 min, 8.0 J cm^{-2})). (D) Absolute CC_{50} values for single versus dual photosensitizer PDT in MCF7 breast cancer cells. CC_{50} values are relative to untreated cells (i.e., no compound or light illumination). Independent samples (n = 3).

https://doi.org/10.1021/acs.jmedchem.2c01504
J. Med. Chem. 2022, 65, 16679−16694

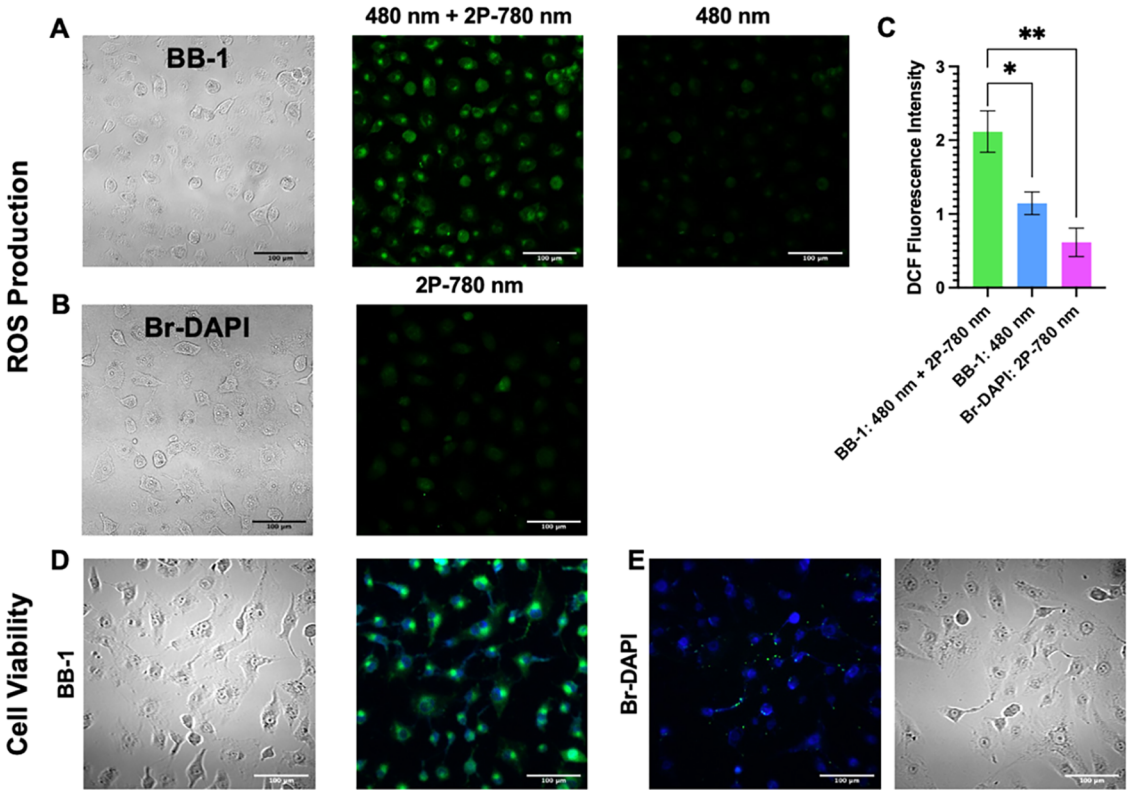

Figure 7. Two-photon (2P) ROS production in MCF7 cells by (A) **BB-1** (3 μM) after 480 nm illumination (15 min, 2.3 J cm^{-2}) + 780 nm 2P illumination (10 s, 16 J) (left) or 480 nm illumination (right), compared to (B) Br-DAPI (3 μM) with 780 nm 2P illumination (10 s, 16 J). ROS monitored by green fluorescence of DCF upon oxidation of $DCFH_2$ (10 μM). (C) Quantification of the mean fluorescence intensity of DCF for each treatment demonstrates a statistically significant difference between dual photosensitization with **BB-1** and single PS illumination. Analyzed by two-tailed *t*-test, *p*-value <0.05 indicated by *. DCF imaged using an Alexa 488 filter set (λ_{ex} = 450−490 nm, λ_{em} = 500−550 nm). MCF7 cells incubated with 4 μM (D) **BB-1** or (E) Br-DAPI, illuminated with a 480 nm light (15 min, 2.3 J cm^{-2}) + 780 nm 2P laser (30 s, 48 J), or a 780 nm 2P laser only (30 s, 48 J), respectively, and then incubated for 2 h and assayed for cell death using ReadyProbes Cell Viability Imaging Kit. Overlay of green nuclear fluorescence with the blue total cell stain is present in more cells treated with **BB-1** compared to Br-DAPI indicating the effectiveness of dual 2P PDT. Independent samples (n = 3). 20× magnification, scale bar = 100 μm. Blue, total cell stain imaged using a DAPI filter set (λ_{ex} = 350−405 nm, λ_{em} = 415−470 nm); green, dead cell stain imaged using an Alexa 488 filter set (λ_{ex} = 450−490 nm, λ_{em} = 500−550 nm).

Figures 6D and S20. Across all three cell lines, **BB-1** exhibited greater photocytotoxicity compared to **BB-2**, and the combination of 480 nm + UV light was more photocytotoxic compared to 480 nm light alone, which is consistent with the higher degree of ROS production. Interestingly, in MCF7 and A549 cells treated with **BB-1**, 480 nm + UV light (i.e., dual photosensitization) versus 480 nm light (i.e., single photosensitization) induced large fold-changes in potency (i.e., 8.5-fold and 17-fold, respectively) suggesting synergistic photocytotoxicity, with lesser synergism observed in HeLa cells (2.2-fold) (Figures 6D and S20). In comparison to Br-DAPI with UV light, the largest enhancement in photocytotoxicity with **BB-1** (480 nm + UV light) was observed in MCF7 cells, whereby **BB-1** was 16-fold more potent (CC_{50} = 0.47 versus 7.6 μM) (Figure 6D). We did not observe this same extent of synergy in A549 and HeLa cells, which is consistent with the lower levels of ROS produced in these cell lines (Figure S20). We hypothesize such observations could be due to differences in cell permeability and defense mechanisms to oxidative stress.[4] We also assayed for dark toxicity due to **BB-1** after a 48 h incubation period in MCF7 cells to demonstrate that minimal dark toxicity occurs under clinical setting ranges (Figure S21).

Although the photocytotoxicity exerted by **BB-1** on MCF7 cells suggests that it is a promising agent for dual PDT, the requirement for UV light is a drawback for *in vivo* PDT applications.[53−55] We previously measured the 2P-absorption cross section of Br-DAPI and found it to have a cross section as high as 2.9 GM at 700 nm.[30] We further demonstrated that 2P illumination at 780 nm can induce a photocytotoxic response in bacteria treated with Br-DAPI, with no background phototoxicity due to light alone.[30] To show that 2P-excitation of Br-DAPI is also applicable to killing cancer cells, we first measured ROS production using $DCFH_2DA$ (10 μM) in MCF7 cells incubated with 3 μM **BB-1** or Br-DAPI. After uncaging **BB-1** (i.e., illuminated with 480 nm light), the cells were imaged for DCF fluorescence before and after illumination with a 780 nm 2P laser (10 s, 16 J). The cells containing **BB-1** and illuminated with both 480 nm light and 780 nm 2P laser showed highest green DCF signals compared to 480 nm illumination only or Br-DAPI treated cells illuminated with a 780 nm 2P laser, consistent with the 1P illumination ROS results (Figure 7A−C). Only minimal background fluorescence from DCF was observed under the same illumination conditions (Figure S22). To determine if the amount of ROS produced using 2P illumination was sufficient to induce cancer cell death, we treated the MCF7 cells with **BB-1** or Br-DAPI (4 μM), followed by illumination with both 480 nm light (15 min, 2.3 J cm^{-2}) and a 780 nm 2P laser (30 s, 48 J) for **BB-1** and a 780 nm 2P laser (30 s, 48 J) only for Br-

https://doi.org/10.1021/acs.jmedchem.2c01504
J. Med. Chem. 2022, 65, 16679−16694

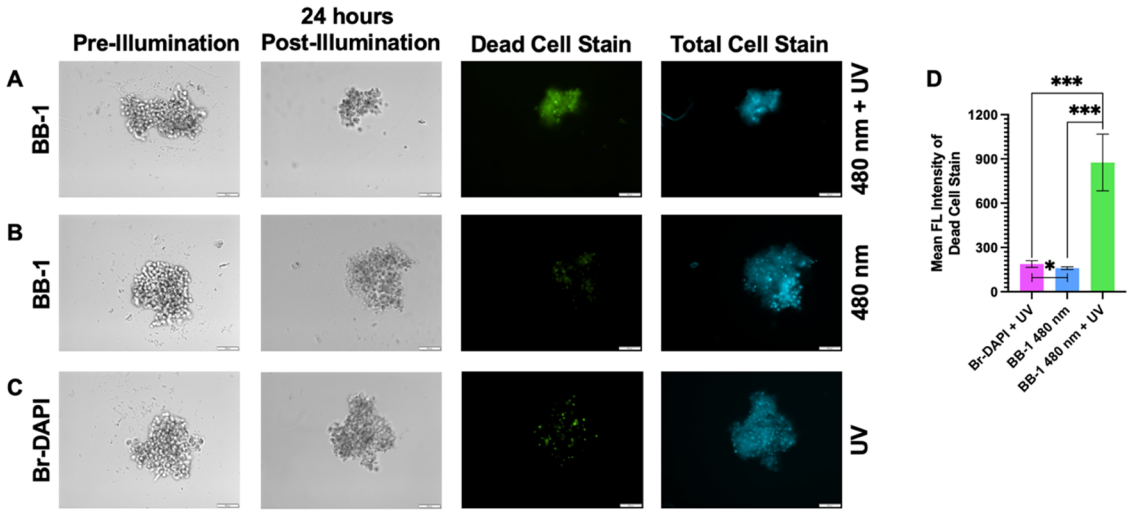

Figure 8. MCF7 tumor spheroids treated with 10 μM **BB-1** (A–B) with (A) 480 nm illumination (15 min, 2.3 J cm^{-2}) + UV (5 min, 8.0 J cm^{-2}), (B) 480 nm illumination (15 min, 2.3 J cm^{-2}, **BB-1**) followed by overnight incubation, or (C) treated with Br-DAPI (10 μM) and UV illumination (5 min, 8.0 J cm^{-2}, Br-DAPI), followed by overnight incubation. Photocytotoxicity was assayed for using ReadyProbes Cell Viability Imaging Kit, where dead cells show green fluorescence, and all cells (live or dead) were stained with blue fluorescence. (D) Relative photocytotoxicity was quantified by plotting the mean fluorescence intensity of the green, fluorescent dead cell stain, where a statistically significant increase in photocytotoxicity was observed in tumor spheroids treated with **BB-1** and dual PDT. Analyzed by two-tailed *t*-test, *p*-value <0.05 indicated by *. Independent samples (n = 6). 10× magnification, scale bar = 100 μm. Blue, total cell stain imaged using a DAPI filter set (λ_{ex} 350–405 nm, λ_{em} 415–470 nm); green, dead cell stain using an EGFP filter set (λ_{ex} 450–495 nm, λ_{em} 500–550 nm).

DAPI. Staining the cells 2 h post-illumination with ReadyProbes Cell Viability Imaging Kit showed more green fluorescence (i.e., dead cells) overlayed with the blue, fluorescent total cell stain (i.e., live and dead cells) for **BB-1** treated MCF7 cells compared to Br-DAPI (Figure 7D,E), with no cell death due to light illumination only (Figure S22). Moreover, **BB-1** induced a concentration-dependent photocytotoxic response with 2P illumination (Figure S23), thus suggesting that 2P-induced cell death in combination with 480 nm uncaging/photosensitization can overcome the UV light penetration limitations *in vivo*.

Photocytotoxicity Measurements in MCF7 Breast Cancer Tumor Spheroids. Photocytotoxicity measured using cells grown in two-dimensional (2D) monolayers are beneficial due to ease of application and the ability to control microenvironmental factors; however, they are not reliable predictors for *in vivo* models.[56,57] To get a better representation of how **BB-1** would perform *in vivo*, we generated MCF7 tumor spheroids which proliferate more similarly to patient tumor tissues and better resemble the complex tumor microenvironment.[56,57] MCF7 cells were grown into spheroids (~300 μm diameter) using ultralow attachment plates. We first confirmed that **BB-1** and Br-DAPI were still able to penetrate the cells by incubating spheroids with 10 μM **BB-1** or Br-DAPI in the dark overnight and imaging for the green and cyan fluorescence from WinterGreen and Br-DAPI, respectively. Strong fluorescent signals above background were observed for both compounds, with minimal cyan fluorescence (i.e., Br-DAPI) in **BB-1** treated spheroids, which is expected given its lack of nuclear entry and good hydrolytic stability (Figure S24). To assess the photocytotoxicity toward MCF7 spheroids, **BB-1** or Br-DAPI were added to the media (final concentration 10 μM), incubated for 1 h, then, **BB-1** treated spheroids were illuminated with 480 nm light (15 min, 2.3 J cm^{-2}) only, or 480 nm light (15 min, 2.3 J cm^{-2}) followed by a UV lamp (5 min, 8.0 J cm^{-2}), while Br-DAPI treated spheroids were illuminated with a UV lamp only (5 min, 8.0 J cm^{-2}). After overnight incubation, MCF7 spheroids treated with **BB-1** and dual illumination showed green fluorescence (dead cells) throughout the entire spheroid and a notable reduction in the tumor spheroid size (~5× smaller in diameter) (Figure 8A). In contrast, spheroids treated with only one PS illumination wavelength (i.e., 480 nm light or UV light) showed significantly fewer green, fluorescent cells and no decrease in spheroid size (Figure 8B,C). Despite the number of cells per spheroid being different after treatment, there were significantly more dead cells in the intact spheroids after treatment with **BB-1** and 480 nm + UV illumination, even with tumor spheroid shrinkage observed.

CONCLUSIONS

In summary, we have shown PDT efficacy can be enhanced using nuclear and cytosolic targeted PSs as a single agent (i.e., **BB** conjugate: Br-DAPI linked to WinterGreen photocage). Our report of **BB** is the first design of a small-molecule PS with well-defined nuclear targeting whereby nuclear entry can be photo-controlled using a photosensitizing photocage for dual-targeted PDT. Compared to Br-DAPI as a stand-alone PS, **BB** conjugates enhanced cell permeability, ROS production, and photocytotoxicity in breast, lung, and cervical cancer cells. In 2D cancer cell monolayers, **BB-1** showed a 16-fold more potent CC_{50} in MCF7 breast cancer cells compared to Br-DAPI alone, suggesting nuclear/cytosolic targeted PDT is an effective strategy. In addition, extensive cell death throughout the cells in three-dimensional (3D) tumor spheroids, as well as tumor spheroid shrinkage was observed. The **BB** conjugates could be excited using 2P light in mammalian cells, which is beneficial for deeper tissue penetration depth and minimal phototoxicity from light alone. To accurately prove that our method for dual-targeted PDT is more effective relative to using a single PS, we performed all experiments with our conjugate and compared it to its individual PS moieties. The

https://doi.org/10.1021/acs.jmedchem.2c01504
J. Med. Chem. 2022, 65, 16679–16694

potential for synergistic photocytotoxicity from photosensitization using this single agent opens new avenues for enhancing PDT efficacy since our approach uses a PS that specifically targets DNA, and the other PS region can easily be changed for optimization of this dual-targeted approach.

We note that several modifications/improvements will be explored with future **BB**-conjugates: (i) Though the photocage/PS localized mainly in the cytosol, it may be possible to install a PS targeted to mitochondria only for examining the efficacy of a nuclear and mitochondria single PDT agent; (ii) the use of longer wavelength PS/photocages is also possible (e.g., red light) to be combined with the 2P-excitability from Br-DAPI for *in vivo* applications; (iii) finally, as Br-DAPI contains another aryl amidine site, it may be possible to install an enzyme trigger group to achieve cancer-selectivity since the nuclear ROS produced by **BB** probes have the potential to damage healthy cells and/or induce formation of new tumors upon light exposure.[58] This will assist in potential clinical applications to be more effective in treating cancers without affecting surrounding healthy tissues. Such modifications are currently being explored so that future *in vivo* work is done using an optimized Br-DAPI-photosensitizer conjugate.

EXPERIMENTAL SECTION

Materials and General Methods. All chemicals and instruments were obtained from commercial suppliers. NMR data was obtained using a 400 MHz Bruker Advance III NMR Spectrometer and HRMS data acquired on an Agilent 6538 UHD, both at the University of Toronto. All final probes were purified using reverse-phase, high-performance liquid chromatography (RP-HPLC) on an LC-20AT Shimadzu liquid chromatograph, equipped with an SPD-M20A VD diode array detector and CBM-20A VP system controller, using a C18 semi-prep column (250 mm × 10 mm). *In vitro* assays were all performed in PBS pH 7.4 (1×) (Ref# 10010-023, purchased from Fisher Scientific). UV−Vis absorption experiments were recorded on a Shimadzu UV-1800 spectrometer and fluorescence experiments were recorded on a Shimadzu RF-6000 spectrometer (purchased from Mandel Scientific Company, Inc.). All samples run on the spectrometers were first added to a 1.0 cm path length quartz cuvette (purchased from Starna Scientific Ltd.) with a 60 μL working volume. One photon (1P) illumination experiments were conducted using an Olympus IX73 inverted microscope containing a mercury lamp equipped with a 450−495 nm excitation filter from an EGFP fluorophore filter set (N2713500, purchased from Olympus Corporation) with an irradiance of 2.5 mW cm^{-2}, UV lamp (UVP BLAK B100APR Lamp, 100 W, 365 nm, 115 V-60 Hz, high-intensity UV lamp, purchased from Analytik Jena GmbH), or 490 nm LED (26 nm bandwidth, 240 mW LED output power; 2.5 μW mm^{-2}, maximum irradiance; M490L4, purchased from ThorLabs). Two-photon (2P) illumination experiments were conducted using an LSM880 confocal microscope equipped with an InSightX3+ Tunable Laser (pulse width <120 fs, beam diameter 1.1 ± 0.2 mm).

Synthetic Procedures. ***Br-DAPI*** *(Synthesized as Previously Reported[9]).* 4′,6-Diamidino-2-phenylindole dihydrochloride (purchased from Biosynth Carbosynth, 1 equiv, 0.0100 g, 0.029 mmol) was dissolved in a mixture of distilled water/acetone (1 mL total volume, 1:1). Next, *N*-bromosuccinimide (3 equiv, 0.0154 g, 0.087 mmol) was added, and the reaction mixture was stirred overnight at room temperature protected from light. The crude mixture was dried under reduced pressure and purified directly by RP-HPLC in ACN (containing 0.1% formic acid) in Milli-Q water (45 min method with a 25 min gradient from 5 to 100% ACN, monitored at 345 nm); product elutes at 21 min peak during the gradient. Br-DAPI was obtained as a yellow solid with 45% yield (0.0046 g, 0.013 mmol). Purity is >95%. HRMS (ESI+) *m*/*z* calculated for $C_{16}H_{14}BrN_5$ 355.04; [M + H]$^+$ found at 356.0500. ^{1}H NMR (400 MHz, d_6-DMSO) δ 8.46 (s, 2H), 8.13 (d, 8.3 Hz, 2H), 8.01 (s, 1H), 7.98 (d, 4.3 Hz, 2H), 7.67 (d, 8.4 Hz, 1H), 7.56 (d, 8.5 Hz, 1H). ^{13}C NMR (101 MHz, d_6-DMSO) δ 168.62, 167.13, 166.07, 137.08, 135.49, 135.28, 131.56, 129.51, 128.73, 123.95, 120.00, 119.56, 113.19, 89.60. See Figures S25−S28.

WinterGreen Photocage. 4,4′-Dimethyl-8-hydroxymethyl-1,3,5,7-tetramethyl-4-bora-3a,4a-diaza-s-indacene was synthesized as previously reported.[59]

4-Nitrophenyl Carbonate WinterGreen. WinterGreen alcohol (1 equiv, 0.027 g, 0.10 mmol) was purged under argon and dissolved in anhydrous dichloromethane (DCM, 7.8 mL). *N*,*N*-Diisopropylethylamine (DIPEA, 3.4 equiv, 0.05 mL, 0.34 mmol) was then added to the mixture and cooled to 0 °C. In a separate flask purged with argon, 4-nitrophenyl chloroformate (3.4 equiv, 0.069 g, 0.34 mmol), anhydrous DCM (3.9 mL), and pyridine (3.4 equiv, 0.03 mL, 0.34 mmol) were mixed to form a cloudy white solution. The 4-nitrophenyl chloroformate solution was then added dropwise to WinterGreen alcohol while maintaining the temperature at 0 °C. The reaction was protected from light and stirred at room temperature for 4 h, where the color changed from red to burgundy upon completion. The solvent was removed under reduced pressure and purified using silica column chromatography in a gradient of hexanes to 20% ethyl acetate (product elutes as first red band). 4-Nitrophenyl carbonate WinterGreen was obtained as a red solid in 87% yield (0.038 g, 0.09 mmol). HRMS (ESI+) *m*/*z* calculated for $C_{23}H_{26}BN_3O_5$ 435.20; [M + H]$^+$ found at 436.2041. ^{1}H NMR (400 MHz, chloroform-*d*) δ 8.28 (d, 5.92 Hz, 2H), 7.39 (d, 5.92 Hz, 2H), 6.12 (s, 2H), 5.61 (s, 2H), 2.48 (s, 6H), 2.46 (s, 6H), 0.20 (s, 6H). ^{13}C NMR (400 MHz, chloroform-*d*) δ 155.19, 153.66, 152.13, 136.75, 130.99, 130.71, 125.21, 122.98, 121.44, 62.47, 16.47, 15.90. See Figures S29−S31.

*BB Probes (**BB-1** and **BB-2**).* Br-DAPI (1 equiv, 0.020 g, 0.056 mmol) was dried down to a flask, purged with argon, and dissolved in anhydrous *N*,*N*-dimethylformamide (DMF, 0.5 mL). Triethylamine (6 equiv, 0.08 mL, 0.34 mmol) was then added, and the mixture turned brighter yellow. 4-Nitrophenyl carbonate WinterGreen (1 equiv, 0.024 g, 0.056 mmol) was dissolved in anhydrous DMF (1 mL) and added dropwise to the Br-DAPI solution. The reaction mixture was stirred overnight at 40 °C while being protected from light. After solvent removal under reduced pressure, the Br-DAPI-WinterGreen conjugates (**BB-1** and **BB-2**; conformational isomers where **BB-1** has the photocage attached to the phenylindole amidine and **BB-2** has the photocage attached to the phenyl amidine) were purified directly by RP-HPLC in using a gradient of ACN (containing 0.1% formic acid) and Milli-Q water (60 min method, 25 min gradient, hold 100% ACN for 15 min). **BB-1** elutes at 33 min peak (15% yield; 0.005 g, 0.008 mmol) and **BB-2** elutes at 31 min peak (12% yield; 0.004 g, 0.007 mmol), both in 100% ACN to yield orange-pink solids. Purity is >95% for **BB-1** and **BB-2**. HRMS (ESI+) *m*/*z* calculated for $C_{33}H_{35}BBrN_7O_2$ 651.52; [M + H]$^+$ found at 652.2209 and 652.2219 for **BB-1** and **BB-2**, respectively. See Figures S32−S37.

BB-1. ^{1}H NMR (500 MHz, d_6-DMSO) δ 9.35 (s, 1H), 8.44 (s, 1H), 8.28 (d, 9.06 Hz, 1H), 8.18 (d, 7.94 Hz, 2H), 8.03 (d, 7.94 Hz, 2H), 7.94 (s, 1H), 7.69 (d, 8.70 Hz, 1H), 7.58 (d, 8.46 Hz, 1H), 7.42 (d, 9.06 Hz, 1H), 6.23 (s, 2H), 5.34 (s, 2H), 2.43 (s, 6H), 2.38 (s, 6H), 0.15 (s, 6H). ^{13}C NMR (500 MHz, d_6-DMSO) δ 166.78, 163.75, 152.77, 137.61, 137.34, 135.11, 134.46, 133.85, 131.56, 131.08, 128.65, 128.12, 127.98, 125.41, 123.35, 122.96, 119.97, 119.37, 112.92, 89.21, 58.81, 16.55, 15.80, 10.42.

BB-2. ^{1}H NMR (500 MHz, d_6-DMSO) δ 9.33 (s, 1H), 8.37 (s, 1H), 8.20 (s, 1H), 8.10 (d, 8.46 Hz, 2H), 7.97 (d, 8.45 Hz, 2H), 7.85 (d, 8.58 Hz, 1H), 7.53 (d, 8.48 Hz, 1H), 6.22 (s, 2H), 5.33 (s, 2H), 2.43 (s, 6H), 2.38 (s, 6H), 0.14 (s, 6H). ^{13}C NMR (500 MHz, d_6-DMSO) δ 167.36, 165.27, 165.05, 163.10, 152.04, 136.95, 135.24, 134.61, 130.43, 130.07, 128.73, 127.93, 127.77, 125.95, 122.26, 119.81, 118.01, 112.23, 88.96, 58.03, 46.70, 15.88, 15.13, 11.68, 9.76.

Br-DAPI Methyl Carbamate. Br-DAPI (1 equiv, 0.006 g, 0.017 mmol) was dissolved in 3:1 tetrahydrofuran (THF)/water (0.6 mL total volume). K_2CO_3 (6 equiv, 0.014 g, 0.10 mmol) and methyl chloroformate (1.2 equiv, 1.9 mg, 0.020 mmol) were then added, and the reaction mixture was stirred at 0−5 °C for 1 h (reaction progression monitored by thin-layer chromatography (TLC)). The

https://doi.org/10.1021/acs.jmedchem.2c01504
J. Med. Chem. 2022, 65, 16679−16694

crude mixture was filtered, and the solvent removed under reduced pressure. The residue was purified directly by RP-HPLC in ACN (containing 0.1% formic acid) in Milli-Q water (55 min method with a 25 min gradient from 5 to 100% ACN, hold 100% ACN for 10 min, monitored at 345 nm); product elutes at 25 min peak during the gradient. Br-DAPI methyl carbamate (0.004 g, 0.001 mmol) was obtained as a white solid in 57% yield. HRMS (ESI+) m/z calculated for $C_{18}H_{17}BrN_5O_2$ 413.05; $[M + H]^+$; found 414.0567. ^{1}H NMR (500 MHz, d_6-DMSO) δ 12.35 (s, 1H), 9.15 (s, 5H), 8.26 (s, 1H), 8.17 (m, 3H), 8.03 (d, 8.34 Hz, 2H), 7.80 (d, 8.37 Hz, 1H), 7.54 (d, 8.52 Hz, 1H), 3.65 (s, 3H), 3.64 (s, 3H). ^{13}C NMR (500 MHz, d_6-DMSO) δ 136.45, 135.44, 134.51, 134.04, 130.74, 129.46, 128.45, 128.08, 120.21, 118.58, 112.64, 89.11, 52.30. See Figures S38−S41.

***In Vitro* Experiments.** *Preparation of Stock Solutions and Concentration Measurements.* Stock solutions of key compounds were prepared in assay-grade DMSO (D12345, purchased from Fisher Scientific). A stock solution of calf thymus DNA (CT-DNA, purchased from Sigma-Aldrich) was prepared in 10 mM Tris buffer containing 1 mM EDTA, pH 8.0. Concentrations of key compounds were measured in PBS pH 7.4 using previously reported molar extinction coefficients. Br-DAPI (33 000 M^{-1} cm^{-1} at 353 nm)[1] and **BB** probes using the extinction coefficient for the reported BODIPY compound (68 500 M^{-1} cm^{-1} at 512 nm).[2] The estimated molecular weight of CT-DNA (652 g mol^{-1}) was used to prepare a 0.5 mM stock solution in ultrapure distilled water.[3]

Parallel Artificial Membrane Permeability Assay (PAMPA). The PAMPA data was acquired from Dalriada Drug Discovery using their standard protocol. The basic setup consisted of the acceptor plate (MultiScreen IP Filter Plate) and the donor plate (96-well Collection Plate) (both purchased from Millipore Sigma), separated by an artificial membrane prepared from 15 mg mL^{-1} L-α-lecithin (from egg yolk, purchased from Sigma-Aldrich) in a solution of 40% chloroform and 60% dodecane. The artificial membrane mixture (7 μL) was added into each acceptor plate well (top compartment), followed by the addition of 300 μL each of PBS pH 7.4 (containing 5% DMSO) and the drug-containing donor solutions (50 μM compound in PBS pH 7.4, containing 5% DMSO) to each well of the donor plate (bottom compartment). The acceptor plate was placed into the donor plate and incubated at r.t. for 16 h in the dark. After incubation, 10 μL aliquots from each well of the acceptor and donor plate were transferred into a new 96-well plate. To each well, 190 μL of ACN (containing 300 nM dexamethasone and 100 nM phenacetin) was added into each well. The plate was then vortexed at 750 rpm for 2 min and centrifuged at 7000g for 10 min. The concentrations of the compounds were determined by LC/MS/MS, with the effective permeability (P_e) in cm s^{-1}, calculated using eq 1. Experiment performed in triplicate using independent samples.

$$-\mathrm{Log}\,P_e = \log\left\{C \times \left[-\ln\left(1 - \frac{[\mathrm{drug}]_{\mathrm{acceptor}}}{[\mathrm{drug}]_{\mathrm{equilibrium}}}\right)\right]\right\} \quad (1)$$

Absorption Spectra. The absorbance spectra of **BB-1**, **BB-2**, Br-DAPI, WinterGreen photocage, and Br-DAPI methyl carbamate were measured in PBS pH 7.4 (60 μL total volume) and normalized to 1 at their absorbance maximum.

Fluorescence Spectra. The fluorescence spectra of **BB-1**, **BB-2**, and Br-DAPI were measured in PBS pH 7.4 (60 μL total volume), where their absorbance at 345 nm (i.e., excitation wavelength) were matched to be 0.525. This was also repeated using Br-DAPI methyl carbamate and Br-DAPI, with their absorbances matched at 345 nm to be 0.517. To each sample, CT-DNA was added for a final concentration of 60 μM and the fluorescence spectrum was measured again. Fluorometer parameters: λ_{ex} 345 nm (1.5 nm slit), λ_{em} 350−650 nm (3.0 nm slit), 600 nm min^{-1} scan speed, high sensitivity.

Binding Affinity to CT-DNA. To a solution of **BB-1**, **BB-2**, or Br-DAPI (20 μM) in PBS pH 7.4 (60 μL total volume), CT-DNA was titrated into samples at increasing concentrations (increments of 10 μM). The fluorescence spectrum of the compound after each CT-DNA addition was measured until the fluorescence plateaued (~60 μM). The K_D values for compounds were determined using a fitting equation on GraphPad Prism for one-site total saturation binding, which assumes any nonspecific binding is proportional to the concentration of ligand. Fluorometer parameters: λ_{ex} 345 nm (1.5 nm slit), λ_{em} 350−650 nm (3.0 nm slit), 600 nm min^{-1} scan speed, high sensitivity. Experiment performed in triplicate using independent samples.

Binding Affinity of WinterGreen Photocage Region (i.e., BODIPY Moiety) to CT-DNA. To a solution of **BB-1** (20 μM) in PBS pH 7.4 (60 μL total volume), CT-DNA was titrated into the sample at increasing concentrations (increments of 10 μM, up to 50 μM). The absorbance spectrum of the compound after each CT-DNA addition was measured and the WinterGreen photocage (i.e., BODIPY moiety) of the spectra were plotted. Experiment performed in triplicate using independent samples.

Singlet Oxygen Quantum Yield (Φ_Δ) of WinterGreen Photocage. The singlet oxygen quantum yield was determined using 1,3-diphenylisobenzofuran (DPBF)[4] (105481, purchased from Sigma-Aldrich). A solution of WinterGreen photocage (absorbance at 490 nm = 0.162) and DPBF (50 μM from a 50 mM stock in ethanol) in 1:1 D_2O/ethanol mixture (60 μL total volume) was prepared and illuminated using a 490 nm LED (12 mW cm^{-2}). The absorbance spectrum was measured initially and then every 20 s in between illuminations, for 1 min total time. The experiment was repeated using Eosin Y as a standard photosensitizer (Φ_Δ = 0.42 in methanol[5]), with its absorbance matched to that of WinterGreen photocage at 490 nm (i.e., 0.162). Equation 2 was used to calculate the Φ_Δ of WinterGreen photocage to be 0.42 ± 0.03. Experiment performed in triplicate using independent samples.

$$\phi_\Delta = \phi_{\Delta,\mathrm{std}}(1 - 10^{-A_{\mathrm{std}}}/1 - 10^{-A})\left(\frac{m}{m_{\mathrm{std}}}\right) \quad (2)$$

where A is the absorbance and m is the slope of the DPBF photobleaching curve at 400 nm.

Fluorescence Analysis of Photo-Uncaging Products. Solutions containing Br-DAPI, **BB-1**, or **BB-2** (1 μM) and CT-DNA (60 μM) in PBS pH 7.4 (60 μL total volume) were prepared and their fluorescence spectrum was measured. Samples containing **BB** probes were then illuminated for 20 min using a 480 nm light (3.1 J cm^{-2}), followed by another fluorescence scan, where their fluorescence intensities at 450 nm were compared to that of Br-DAPI at the same concentration to confirm the release of Br-DAPI from WinterGreen photocage. Fluorometer parameters: λ_{ex} 345 nm (1.5 nm slit), λ_{em} 350−650 nm (3.0 nm slit), 600 nm min^{-1} scan speed, high sensitivity. Experiment performed in triplicate using independent samples.

Analytical RP-HPLC Analysis of Photo-Uncaging Products. Each sample (Br-DAPI, **BB-1**, and **BB-2** incubated in the dark, and **BB-1** and **BB-2** after photo-uncaging) (50 μM) were analyzed by RP-HPLC using a C18 analytical column (250 mm × 3 mm). The samples to test for the stability of **BB** probes toward hydrolysis were prepared by incubating each compound in PBS pH 7.4 (30 μL total volume) in a water bath maintained at 37 °C for 3 h in the dark. The samples to test for the photo-uncaging products were prepared in PBS pH 7.4 (30 μL total volume) and illuminated using 480 nm light for 20 min (3.1 J cm^{-2}). All samples were run in a gradient of ACN (containing 0.1% formic acid) and Milli-Q water (65 min method, 25 min gradient, hold 100% ACN for 20 min). The identities of each sample were confirmed by comparing their relative retention times absorbance spectra, and HRMS of collected peak for the photo-uncaged product to those of Br-DAPI, to confirm probe stability and Br-DAPI release after illumination conditions for uncaging. Experiment performed in duplicate using independent samples.

Photostability of WinterGreen Photocage toward Photo-Uncaging Illumination. A solution containing **BB-1** (absorbance at 490 nm = 0.440) in PBS pH 7.4 (60 μL total volume) was illuminated using a 490 nm LED (12 mW cm^{-2}), with the absorbance spectrum was measured initially (i.e., before illumination) and then every 5 min after for 15 min total. Experiment performed in triplicate using independent samples.

https://doi.org/10.1021/acs.jmedchem.2c01504
J. Med. Chem. 2022, 65, 16679−16694

Aqueous Stability of BB Probes (i.e., Hydrolysis Test). Solutions containing 0.8 μM **BB-1** or **BB-2** and 60 μM CT-DNA were prepared in PBS pH 7.4 (80 μL total volume) and incubated in a water bath at 37 °C for 3 h in the dark. The fluorescence spectrum of each sample was measured at time 0 and 3 h after incubation, where the fluorescence at 450 nm was compared at each time point to confirm stability of the carbamate linkage toward spontaneous hydrolysis and release of Br-DAPI. Fluorometer parameters: λ_{ex} 345 nm (1.5 nm slit), λ_{em} 350−650 nm (3.0 nm slit), 600 nm min^{-1} scan speed, high sensitivity. Experiment performed in triplicate using independent samples.

ROS Production Monitored by DCFH$_2$In Vitro. Solutions containing 1 μM **BB-1**, **BB-2**, or Br-DAPI, and 1 μM DCFH$_2$ (0.6 μL from a 100 μM stock prepared from a 10 mM DCFH$_2$-DA in 0.1 M NaOH$_{(aq)}$) were prepared in PBS pH 7.4 (60 μL total volume). Br-DAPI samples were illuminated with a UV lamp (8.0 J cm^{-2}) for 5 min or a 2P laser at 780 nm (48 J) for 30 s. **BB-1** or **BB-2** samples were illuminated with a 480 nm light (2.3 J cm^{-2}) for 15 min, 480 nm light (2.3 J cm^{-2}) for 15 min + a UV lamp (8.0 J cm^{-2}) for 5 min, or 480 nm light (2.3 J cm^{-2}) for 15 min + 2P laser at 780 nm (48 J) for 30 s. The fluorescence of DCF for each sample was measured immediately after illumination. Background from the sensor was measured using samples containing 1 μM DCFH$_2$ in PBS pH 7.4 under each illumination condition used above. Statistical analyses were conducted using an unpaired *t*-test to determine the *p*-values between different compounds and under different illumination conditions. Fluorometer parameters: λ_{ex} 505 nm (1.5 nm slit), λ_{em} 510−545 nm (3.0 nm slit), 600 nm min^{-1} scan speed, low sensitivity. Experiment performed in triplicate using independent samples. *Note that the DCF fluorescence with **BB** compounds under dark conditions could not accurately be measured because the excitation/emission parameters of **BB** (before being photobleached during illumination) overlap with that of DCF.

DNA Photo-Cleavage Facilitated by ROS Produced by BB Probes and Br-DAPI Monitored by Agarose Gel Electrophoresis. Samples containing 70 ng of circular, plasmid DNA (pCMV-PARP1−3xFlag-WT, 7146 bp length; purchased from Addgene) only or 10 μM Br-DAPI, **BB-1**, or **BB-2**, were prepared in PBS pH 7.4 (10 μL total volume) in transparent Eppendorf tubes. Samples designated for light treatment were illuminated with a UV lamp (8.0 J cm^{-2}) for 5 min (plasmid only and Br-DAPI) or 480 nm light (2.3 J cm^{-2}) for 15 min + a UV lamp (8.0 J cm^{-2}) for 5 min (plasmid only, **BB-1**, and **BB-2**). After illumination, 1 μL of a 2 M NaOH$_{(aq)}$ solution (containing 0.1 M EDTA) was added, and samples were denatured in a 90 °C water bath for 1 min. After cooling samples on ice, 3 μL of the loading buffer was added (50% sucrose/bromophenol blue solution; total sample volume 15 μL). A 1% agarose gel containing 0.5 mg mL^{-1} ethidium bromide was prepared in 1× TBE buffer. Each sample (15 μL) was added to individual wells, and the gel was run in TBE buffer at 100 V for 80 min on a Mini-SubCell GT Cell (purchased from Bio-Rad Laboratories). When complete, the gel was washed two times with Milli-Q water and imaged using an Invitrogen iBright 1500 Imaging System (purchased from Fisher Scientific). Damaged DNA was visualized using the ethidium bromide channel, where the bands representing intact plasmid was assigned to be linear (top), supercoiled (middle), and open circular (bottom).[50] Experiment performed in duplicate using independent samples.

***In Cellulo* Experiments.** *Cell Culture.* MCF7 (human breast/mammary gland epithelial adenocarcinoma), A549 (human lung epithelial carcinoma), and HeLa (human uterus/cervix epithelial adenocarcinoma) were purchased from American Type Culture Collection (ATCC). Adherent cells were cultured in 75 cm^2 flasks with Nunclon Delta surface treatment (156499, purchased from Fisher Scientific) at 37 °C with 5% CO_2 in a humidified incubator. A549 and HeLa cells were cultured in Dulbecco's modified Eagle's medium with sodium pyruvate (DMEM w/, 319005481) and MCF7 cells were cultured in Dulbecco's modified Eagle's medium without sodium pyruvate (DMEM w/o, 319015105) (both purchased from WISENT, Inc.). Both media were supplemented with 10% fetal bovine serum (A31607-02, purchased from Fisher Scientific) and 1% antibiotic-antimycotic solution (450-115-EL, purchased from WISENT, Inc.). Incubation of cells with compounds was done in OPTI-MEM 1× reduced serum medium (31985-062) while washes and imaging were done using Dulbecco's phosphate buffered saline (D-PBS) 1× without calcium and magnesium (311425188) (both purchased from WISENT, Inc.). Cell viability experiments were performed in Nunc MicroWell 96-Well Microplates (cat. 167008, purchased from Fisher Scientific), 1P imaging in 8-well Chambered Coverglass w/ nonremovable wells made with borosilicate glass 1.0 bottom (cat. 155411, purchased from Fisher Scientific), and 2P imaging with 35 mm confocal dishes with 20 mm glass bottom, surface treated (Ref# 734−2904, purchased from VWR).

Intracellular Localization of Compounds with MitoTracker Red. A 1 mM stock solution of MitoTracker Red FM (cat. M22425) was prepared in assay-grade DMSO. MCF7, A549, and HeLa cells were seeded at a concentration of 30 000 cells well^{-1} in growth media and cultured overnight at 37 °C with 5% CO_2. The old media was removed and replaced with **BB-1**, **BB-2**, or Br-DAPI (2 μM) in OPTI-MEM (250 μL) and incubated at 37 °C with 5% CO_2 for 1 h. The media was removed, and the cells were washed once with D-PBS. Next, MitoTracker Red FM (0.5 μM) was added to cells in D-PBS (250 μL) and incubated for 15 min at 37 °C. The PBS was removed, the cells were washed once with D-PBS, and then fresh D-PBS (250 μL) was added in for imaging. The fluorescence from each compound was overlayed with that of MitoTracker Red FM, where yellow fluorescence indicates colocalization. The fluorescence of WinterGreen from **BB-1** and **BB-2** was captured using an EGFP filter set (λ_{ex} = 450−495 nm, λ_{em} = 500−550 nm, bandpass emission), with 500 ms integration time, 1% excitation power, 60× magnification. Br-DAPI fluorescence was captured using a DAPI filter set (λ_{ex} = 350−405 nm, λ_{em} = 415−470 nm, bandpass emission), with 500 ms integration time, 1% excitation power, 60× magnification. MitoTracker Red FM fluorescence was captured using a custom filter set (λ_{ex} = 490−555 nm, λ_{em} = 590−710 nm, bandpass emission), with 250 ms integration time, 1% excitation power, 60× magnification. Experiment performed in triplicate using independent samples.

Br-DAPI Photo-Uncaging from BB Probes Monitored by Fluorescence In Cellulo. MCF7, A549, and HeLa cells were seeded at a concentration of 30 000 cells well^{-1} in growth media and cultured overnight at 37 °C with 5% CO_2. The old media was removed and replaced with **BB-1**, **BB-2**, or Br-DAPI (2 μM) in OPTI-MEM (250 μL) and incubated at 37 °C with 5% CO_2 for 1 h. The media was removed, the cells were washed once with D-PBS, and then D-PBS was added to wells for imaging. The fluorescence from Br-DAPI and WinterGreen were taken at time 0 min (i.e., dark) and following 10 min of 480 nm illumination (1.6 J cm^{-2}). Br-DAPI fluorescence was scaled relative to post-illumination and WinterGreen fluorescence was scaled relative to pre-illumination. The fluorescence of WinterGreen from **BB-1** and **BB-2** was captured using an EGFP filter set (λ_{ex} = 450−495 nm, λ_{em} = 500−550 nm, bandpass emission), with 500 ms integration time, 3% excitation power, 40× magnification. Br-DAPI fluorescence was captured using a DAPI filter set (λ_{ex} = 350−405 nm, λ_{em} = 415−470 nm, bandpass emission), with 500 ms integration time, 1% excitation power, 40× magnification. Experiment performed in triplicate using independent samples.

Intracellular Localization of Br-DAPI Methyl Carbamate. A549 cells were seeded at a concentration of 30 000 cells well^{-1} in growth media and cultured overnight at 37 °C with 5% CO_2. The old media was removed and replaced with Br-DAPI methyl carbamate (~3 μM) and incubated at 37 °C with 5% CO_2 for 1 h. The media was removed, the cells were washed once with D-PBS, and D-PBS was added to the wells for imaging. The fluorescence from Br-DAPI methyl carbamate was captured using a DAPI filter set (λ_{ex} = 350−405 nm, λ_{em} = 415−470 nm, bandpass emission), with 1 s integration time, 1% excitation power, 40× magnification. Experiment performed in triplicate using independent samples.

Stability of BB Probes toward Intracellular Esterases. MCF7, A549, and HeLa cells were seeded at a concentration of 40 000 cells well^{-1} in growth media and cultured overnight at 37 °C with 5% CO_2. The old media was removed and replaced with **BB-1** or **BB-2** (2 μM)

https://doi.org/10.1021/acs.jmedchem.2c01504
J. Med. Chem. 2022, 65, 16679−16694

in OPTI-MEM (250 μL) and incubated at 37 °C with 5% CO_2 for 1 h. The media was removed, the cells were washed once with D-PBS, and then D-PBS was added to wells for imaging. The cyan, fluorescent signal from the **BB** probes were imaged at time 0 and 2 h, with the plate kept at the same position on a heated microscope stage (maintained at 37 °C).

The stability experiment was also repeated under a clinical setting incubation range (i.e., 24 h) with **BB-1** in MCF7 cells. The old media was removed and replaced with **BB-1** (0−2 μM) in OPTI-MEM (250 μL) and incubated at 37 °C with 5% CO_2 for a) 1 h, washed once with D-PBS, and then complete growth media was added to each well for incubation for another 23 h. The old media was removed and then D-PBS was added to wells for imaging of nuclear signals due to Br-DAPI release via intracellular esterases.

The fluorescence was scaled relative to Br-DAPI post photo-uncaging illumination. Br-DAPI fluorescence was captured using a DAPI filter set (λ_{ex} = 350−405 nm, λ_{em} = 415−470 nm, bandpass emission), with 500 ms integration time, 1% excitation power, 20× magnification. Experiment performed in triplicate using independent samples.

1P ROS Production Monitored by DCFH$_2$DA. MCF7, A549, and HeLa cells were seeded at a concentration of 40 000 cells well^{-1} in growth media and cultured overnight at 37 °C with 5% CO_2. The old media was removed and replaced with **BB-1**, **BB-2**, or Br-DAPI (2 μM) in OPTI-MEM (250 μL) and incubated at 37 °C with 5% CO_2 for 1 h. The media was removed, the cells were washed once with D-PBS, followed by the addition of DCFH$_2$DA (10 μM) in D-PBS (250 μL). The cells were incubated at 37 °C for 30 min for intracellular esterases to deacetylate the ROS sensor.[6] The media was removed, the cells were washed once with D-PBS, and then D-PBS was added to the wells for imaging. The cells containing **BB-1** and **BB-2**, were illuminated with a 480 nm light (2.3 J cm^{-2}) for 15 min and the DCF fluorescence imaged. The same cells were illuminated again, except this time using a UV lamp (8.0 J cm^{-2}) for 5 min and the DCF fluorescence imaged again. The cells containing Br-DAPI were illuminated using a UV lamp (8.0 J cm^{-2}) for 5 min and the DCF imaged. The DCF fluorescence for all compounds under different conditions was scaled relative to **BB** probes that had dual illumination (480 nm + UV). The mean DCF fluorescence intensity was quantified using the "Count and Measure" tool and selecting for individual cells on cellSens software. Statistical analyses were conducted using an unpaired *t*-test to determine the *p*-values between different illumination conditions between compounds tested in the same cell line. Controls showing DCF fluorescence with the compounds under dark conditions were not taken because the filter set used for DCF is the same for the WinterGreen region of the **BB** probes. The overlap in fluorescence properties does not affect results for compounds after illumination because WinterGreen photobleaches (i.e., minimal fluorescence) using the photo-uncaging parameters such that all green fluorescence observed is due to DCF only. The fluorescence from DCF (oxidized product of DCFH$_2$)[6] was captured using an EGFP filter set (λ_{ex} = 450−495 nm, λ_{em} = 500−550 nm, bandpass emission), with 500 ms integration time, 1% excitation power, 10× magnification. Experiment performed in triplicate using independent samples.

dsDNA Damage In Cellulo Monitored by γH2A.X Antibody. MCF7 cells were seeded at a concentration of 50 000 cells well^{-1} in growth media and cultured overnight at 37 °C with 5% CO_2. The old media was removed and replaced with 3 μM Br-DAPI or **BB-1** in OPTI-MEM (250 μL) and incubated at 37 °C with 5% CO_2 for 1 h. The media was removed, the cells were washed once with D-PBS, and complete growth media (250 μL) was added into each well. The cells containing Br-DAPI were illuminated with a UV lamp (8.0 J cm^{-2}) for 5 min and those with **BB-1** were illuminated with a 480 nm light (2.3 J cm^{-2}) for 15 min followed by a UV lamp (8.0 J cm^{-2}) for 5 min. After a 2-h incubation at 37 °C with 5% CO_2, the cells were treated with a γH2A.X Staining Kit (ab242296; purchased from Abcam). The cells were washed once with PBS-tween, fixed at 0 °C for 20 min in cold methanol, and washed once more with PBS-tween. Next, blocking buffer (PBS containing 1% bovine serum albumin (BSA)) was added, and the cells were incubated for 30 min at r.t. γH2A.X-Alexa 488 solution (1×) was added to each well (1 μL of γH2A.X in 249 μL of PBS-tween), incubated for 1 h at r.t., and then washed three times with PBS-tween. The antibody staining and washing protocol were then repeated using a γH2A.X secondary antibody solution (1×). Finally, the cells were stained with nuclei-stain DAPI (0.5 μM) in PBS-tween (250 μL) for 15 min, washed once with PBS-tween, and PBS-tween added to image cells. dsDNA breaks were confirmed by overlaying the fluorescence of γH2A.X-Alexa 488 and DAPI. The fluorescence of γH2A.X-Alexa488 is represented by the color red and DAPI by the color blue. The fluorescence of γH2A.X-Alexa488 was captured using an EGFP filter set (λ_{ex} = 450−495 nm, λ_{em} = 500−550 nm, bandpass emission), with 500 ms integration time, 1% excitation power, 40× magnification. DAPI fluorescence was captured using a DAPI filter set (λ_{ex} = 350−405 nm, λ_{em} = 415−470 nm, bandpass emission), with 50 ms integration time, 1% excitation power, 40× magnification. Experiment performed in triplicate using independent samples.

Photocytotoxicity in 2D Monolayer with 1P Illumination (Dose−Response Curves). MCF7, A549, and HeLa cells were seeded at a concentration of 10 000 cells well^{-1} in growth media and cultured overnight at 37 °C with 5% CO_2. The old media was removed and replaced with **BB-1**, **BB-2**, or Br-DAPI (within a range of 0−64 μM) in OPTI-MEM (100 μL) and incubated at 37 °C with 5% CO_2 for 1 h. The media was removed, the cells were washed once with D-PBS, and complete growth media (100 μL) was added into each well. The cells designated for light conditions containing **BB-1** and **BB-2**, were illuminated with 480 nm light (2.3 J cm^{-2}) for 15 min, or with 480 nm light (2.3 J cm^{-2}) for 15 min followed by a UV lamp (8.0 J cm^{-2}) for 5 min, while cells containing Br-DAPI were irradiated with a UV lamp (8.0 J cm^{-2}) for 5 min. The cells designated for dark conditions and those treated with light were incubated overnight at 37 °C with 5% CO_2. Cell viability was quantified 24 h post treatment using an MTT assay (2 h incubation at 37 °C with 5% CO_2 with 0.5 mg mL^{-1} thiazolyl blue tetrazolium tribromide in growth media), where the absorbance at 560 nm of the MTT compound was used to determine the relative viability of the cells compared to untreated cells (i.e., no compound or light illumination).[7] Dose−response curves were plotted on a logarithmic axis and fitted using a nonlinear fit with a variable slope. Experiment performed in triplicate using independent samples.

2P ROS Production in MCF7 Cells Monitored by DCFH$_2$DA. MCF7 cells were seeded at a concentration of 500 000 cells plate^{-1} in growth media and cultured overnight at 37 °C with 5% CO_2. The old media was removed and replaced with **BB-1** or Br-DAPI (3 μM) in OPTI-MEM (1 mL) and incubated at 37 °C with 5% CO_2 for 1 h. The media was removed, the cells were washed once with D-PBS, followed by the addition of DCFH$_2$DA (10 μM) in D-PBS (1 mL). The cells were incubated at 37 °C for 30 min for intracellular esterases to deacetylate the ROS sensor.[6] The media was removed, the cells were washed once with D-PBS, and then D-PBS was added to the wells for imaging. The cells containing **BB-1** were illuminated with 480 nm light (2.3 J cm^{-2}) for 15 min and the DCF fluorescence imaged. The same cells were illuminated again, except this time using a 2P laser at 780 nm (16 J) for 10 s. and the DCF fluorescence imaged again. The cells containing Br-DAPI were illuminated using a 2P laser at 780 nm (16 J) for 10 s and the DCF imaged. The DCF fluorescence for all compounds under different conditions were scaled relative to **BB-1** that had dual illumination (480 nm + 2P 780 nm). The mean DCF fluorescence intensity was quantified using the "Analyze → Measure" tool in Fiji. Statistical analyses were conducted using an unpaired *t*-test to determine the *p*-values between different illumination conditions between compounds tested in the same cell line. Controls showing DCF with the compounds under dark conditions were not taken because the filter set used for DCF is the same for the WinterGreen region of **BB-1**. The overlap in fluorescence properties does not affect results for compounds after illumination because WinterGreen photobleaches (i.e., minimal fluorescence) using the uncaging parameters such that all green fluorescence observed is due to DCF only. The fluorescence from

https://doi.org/10.1021/acs.jmedchem.2c01504
J. Med. Chem. 2022, 65, 16679−16694

DCF (oxidized product of $DCFH_2$)[6] was captured using an Alexa 488 filter set (λ_{ex} = 450−490 nm, λ_{em} = 500−550 nm, bandpass emission), with 85.3 pinhole, 550 master gain, 10% laser power, 20× magnification. 2P illumination was performed using 10 frames of 1 s 100% laser power, 139 mW at the sample plane with ∼100 fs pulse width, 80 MHz repetition through a 1.0 NA objective lens for ten 1 s frames. Experiment performed in triplicate using independent samples.

Photocytotoxicity in MCF7 Cells with 2P Illumination. MCF7 cells were seeded at a concentration of 500 000 cells $plate^{-1}$ in growth media and cultured overnight at 37 °C with 5% CO_2. The old media was removed and replaced with **BB-1** or Br-DAPI (4 μM) in OPTI-MEM (1 mL) and incubated at 37 °C with 5% CO_2 for 1 h. The media was removed, the cells were washed once with D-PBS, and D-PBS was added to the plates for imaging. The cells containing **BB-1** were illuminated with 480 nm light (2.3 J cm^{-2}) for 15 min, followed by a 2P laser at 780 nm (48 J) for 30 s while those incubated with Br-DAPI illuminated with the 2P laser at 780 nm (48 J) for 30 s. The light-treated cells were left to incubate on the microscope stage for 2 h 90 min post-illumination, and the cell viability was analyzed using ReadyProbes Cell Viability Imaging Kit (cat. R37609, purchased from Fisher Scientific), where the blue stain labels all cells (i.e., total cell stain) and the green stain labels dead cells. The cells were incubated with both cell stains simultaneously for 30 min at 37 °C by adding two drops of each stain directly into the D-PBS already in each plate (without moving the plate's position on the microscope stage). After incubation with the cell viability imaging kit, the green dead fluorescent stain was captured using an Alexa 488 filter set (λ_{ex} = 450−490 nm, λ_{em} = 500−550 nm, bandpass emission), with 600 pinhole, 550 master gain, 6% laser power, 20× magnification. The blue total fluorescent stain was captured using a DAPI filter set (λ_{ex} = 350−405 nm, λ_{em} = 415−470 nm, bandpass emission), with 72 pinhole, 500 master gain, 1% laser power, 20× magnification. 2P illumination was performed using 30 frames of 1 s, 100% laser power, 139 mW at the sample plane with ∼100 fs pulse width, 80 MHz repetition through a 1.0 NA objective lens for thirty 1 s frames. Experiment performed in triplicate using independent samples.

Photocytotoxicity in 3D Tumor Spheroids with 1P Illumination. MCF7 tumor spheroids were grown using the ultralow attachment plate method. The cells were seeded at a concentration of 1000 cells $well^{-1}$ in OPTI-MEM (200 μL) and cultured in Nunclon Sphera 96-well, treated U-shaped bottom microplates (cat. 174 925) for 72 h at 37 °C with 5% CO_2. Spheroid growth was monitored by bright-field images, until spheroids looked compact and had a diameter of ∼300 μm at 10× magnification. The old media (100 μL) was carefully removed and replaced with **BB-1** or Br-DAPI (10 μM) in OPTI-MEM (100 μL, in addition to media remaining in well) and incubated for 1 h at 37 °C with 5% CO_2. Spheroids designated for light treatment were irradiated with 480 nm light (2.3 J cm^{-2}) for 15 min, or with 480 nm light (2.3 J cm^{-2}) for 15 min followed by a UV lamp (8.0 J cm^{-2}) for 5 min, while cells containing Br-DAPI were irradiated with a UV lamp (8.0 J cm^{-2}) for 5 min. Spheroids designated for dark conditions and those treated with light were incubated overnight at 37 °C with 5% CO_2. Cell viability for light-treated cells was analyzed using ReadyProbes Cell Viability Imaging Kit (cat. R37609, purchased from Fisher Scientific), where the blue stain labels all cells (i.e., total cell stain) and the green stain labels dead cells. Spheroids were incubated with cell stains for 15 min at 37 °C by adding 100 μL of a solution containing both stains (2 drops each dye mL^{-1} D-PBS). Dark-treated cells were imaged directly for WinterGreen from **BB-1** and Br-DAPI fluorescence from both **BB-1** and Br-DAPI. After incubation with the cell viability imaging kit, the green dead fluorescent stain was captured using an EGFP filter set (λ_{ex} = 450−495 nm, λ_{em} = 500−550 nm, bandpass emission), with 500 ms integration time, 1% excitation power, 10× magnification. The blue total fluorescent stain was captured using a DAPI filter set (λ_{ex} = 350−405 nm, λ_{em} = 415−470 nm, bandpass emission), with 500 ms integration time, 1% excitation power, 10× magnification. The fluorescence of WinterGreen from **BB-1** was captured using an EGFP filter set (λ_{ex} = 450−495 nm, λ_{em} = 500−550 nm, bandpass emission), with 500 ms integration time, 1% excitation power, 10× magnification. Br-DAPI fluorescence was captured using a DAPI filter set (λ_{ex} = 350−405 nm, λ_{em} = 415−470 nm, bandpass emission), with 500 ms integration time, 1% excitation power, 10× magnification. Experiment performed in triplicate using independent samples.

■ ASSOCIATED CONTENT

Supporting Information

The Supporting Information is available free of charge at https://pubs.acs.org/doi/10.1021/acs.jmedchem.2c01504.

Molecular Formula Strings (CSV)

In vitro photophysical data and photo-uncaging characterization, *in cellulo* fluorescence imaging and cell viability data, synthetic procedures, and compound characterization data (i.e., HRMS and NMR) (PDF)

■ AUTHOR INFORMATION

Corresponding Author

Andrew A. Beharry − *Department of Chemical and Physical Sciences, University of Toronto Mississauga, Mississauga, Ontario L5L 1C6, Canada;* orcid.org/0000-0003-1505-2375; Email: andrew.beharry@utoronto.ca

Authors

Elyse M. Digby − *Department of Chemical and Physical Sciences, University of Toronto Mississauga, Mississauga, Ontario L5L 1C6, Canada*

Seylan Ayan − *Department of Chemical and Physical Sciences, University of Toronto Mississauga, Mississauga, Ontario L5L 1C6, Canada*

Pradeep Shrestha − *Department of Chemistry, Iowa State University, Ames, Iowa 50011, United States;* orcid.org/0000-0003-4166-966X

Elizabeth J. Gehrmann − *Department of Chemistry, Iowa State University, Ames, Iowa 50011, United States*

Arthur H. Winter − *Department of Chemistry, Iowa State University, Ames, Iowa 50011, United States;* orcid.org/0000-0003-2421-5578

Complete contact information is available at: https://pubs.acs.org/10.1021/acs.jmedchem.2c01504

Author Contributions

Experiments were designed by E.M.D. and A.A.B. Synthesis of BB probes and control compounds was performed by E.M.D. and S.A. Synthesis of WinterGreen was performed by P.S. and E.J.G. Manuscript was written by E.M.D. and A.A.B. and edited by S.A. and A.H.W. All authors approved the final version of the manuscript.

Notes

The authors declare no competing financial interest.

■ ACKNOWLEDGMENTS

A.A.B. acknowledges support by NSERC Discovery grant. A.H.W. acknowledges support from NSF grant: CHE 2055335.

■ ABBREVIATIONS USED

CT-DNA, calf thymus DNA; $DCFH_2DA$, 2′,7′-dichlorodihydrofluorescein diacetate; DCF, 2′,7′-dichlorodihydrofluorescin; DNA, deoxyribonucleic acid; HPLC, high-performance liquid chromatography; PDT, photodynamic therapy; PS, photosensitizer; ROS, reactive oxygen species

REFERENCES

(1) Luby, B. M.; Walsh, C. D.; Zheng, G. Advanced Photosensitizer Activation Strategies for Smarter Photodynamic Therapy Beacons. *Angew. Chem.* **2019**, *131*, 2580−2591.

(2) Bacellar, I. O. L.; Tsubone, T. M.; Pavani, C.; Baptista, M. S. Photodynamic Efficiency: From Molecular Photochemistry to Cell Death. *Int. J. Mol. Sci.* **2015**, *16*, 20523−20559.

(3) Castano, A. P.; Demidova, T. N.; Hamblin, M. Mechanisms in Photodynamic Therapy: Part One - Photosensitizers, Photochemistry and Cellular Localization. *Photodiagn. Photodyn. Ther.* **2004**, *1*, 279−293.

(4) Yu, B. P. Cellular Defenses against Damage from Reactive Oxygen Species. *Physiol. Rev.* **1994**, *74*, 139−162.

(5) Mahalingam, S. M.; Ordaz, J. D.; Low, P. S. Targeting of a Photosensitizer to the Mitochondrion Enhances the Potency of Photodynamic Therapy. *ACS Omega* **2018**, *3*, 6066−6074.

(6) Liang, P.; Kolodieznyi, D.; Creeger, Y.; Ballou, B.; Bruchez, M. P. Subcellular Singlet Oxygen and Cell Death: Location Matters. *Front. Chem.* **2020**, *8*, 592941.

(7) Yu, Z.; Pan, W.; Li, N.; Tang, B. A Nuclear Targeted Dual-Photosensitizer for Drug-Resistant Cancer Therapy with NIR Activated Multiple ROS. *Chem. Sci.* **2016**, *7*, 4237−4244.

(8) Laskin, J. D.; Jan, Y. H.; Jetter, M. M.; Guillon, C. D.; Mariano, T. M.; Heck, D. E.; Heindel, N. D. Identification of a Pyranocoumarin Photosensitizer That Is a Potent Inhibitor of Keratinocyte Growth. *Photochem. Photobiol.* **2018**, *94*, 577−582.

(9) Digby, E. M.; Rana, R.; Nitz, M.; Beharry, A. A. DNA Directed Damage Using a Brominated DAPI Derivative. *Chem. Commun.* **2019**, *55*, 9971−9974.

(10) Zhang, P.; Huang, H.; Banjeree, S.; Clarkson, G. J.; Ge, C.; Imberti, C.; Sadler, P. J. Nucleus-Targeted Organoiridium−Albumin Conjugate for Photodynamic Cancer Therapy. *Angew. Chem., Int. Ed.* **2019**, *58*, 2350−2354.

(11) Wen, Y.; Schreiber, C. L.; Smith, B. D. Dual-Targeted Phototherapeutic Agents as Magic Bullets for Cancer. *Bioconjugate Chem.* **2020**, *31*, 474−482.

(12) Hirakawa, K.; Hirano, T.; Nishimura, Y.; Arai, T.; Nosaka, Y. Dynamics of Singlet Oxygen Generation by DNA-Binding Photosensitizers. *J. Phys. Chem. B* **2012**, *116*, 3037−3044.

(13) Schneider-Yin, X.; Kurmanaviciene, A.; Roth, M.; Roos, M.; Fedier, A.; Minder, E. I.; Walt, H. Hypericin and 5-Aminolevulinic Acid-Induced Protoporphyrin IX Induce Enhanced Phototoxicity in Human Endometrial Cancer Cells with Non-Coherent White Light. *Photodiagn. Photodyn. Ther.* **2009**, *6*, 12−18.

(14) Villanueva, A.; Stockert, J. C.; Cañete, M.; Acedo, P. A New Protocol in Photodynamic Therapy: Enhanced Tumour Cell Death by Combining Two Different Photosensitizers. *Photochem. Photobiol. Sci.* **2010**, *9*, 295−297.

(15) Kessel, D.; Reiners, J. J., Jr. Effects of Combined Lysosomal and Mitochondrial Photodamage in a Non Small-Cell Lung Cancer Cell Line: The Role of Paraptosis. *Photochem. Photobiol.* **2017**, *93*, 1502−1508.

(16) Cheng, H.; Zheng, R. R.; Fan, G. L.; Fan, J. H.; Zhao, L. P.; Jiang, X. Y.; Yang, B.; Yu, X. Y.; Li, S. Y.; Zhang, X. Z. Mitochondria and Plasma Membrane Dual-Targeted Chimeric Peptide for Single-Agent Synergistic Photodynamic Therapy. *Biomaterials* **2019**, *188*, 1−11.

(17) Cheng, H.; Fan, J. H.; Zhao, L. P.; Fan, G. L.; Zheng, R. R.; Qiu, X. Z.; Yu, X. Y.; Li, S. Y.; Zhang, X. Z. Chimeric Peptide Engineered Exosomes for Dual-Stage Light Guided Plasma Membrane and Nucleus Targeted Photodynamic Therapy. *Biomaterials* **2019**, *211*, 14−24.

(18) Obaid, G.; Broekgaarden, M.; Bulin, A. L.; Huang, H. C.; Kuriakose, J.; Liu, J.; Hasan, T. Photonanomedicine: A Convergence of Photodynamic Therapy and Nanotechnology. *Nanoscale* **2016**, *8*, 12471−12503.

(19) Navya, P. N.; Kaphle, A.; Srinivas, S. P.; Bhargava, S. K.; Rotello, V. M.; Daima, H. K. Current Trends and Challenges in Cancer Management and Therapy Using Designer Nanomaterials. *Nano Convergence* **2019**, *6*, No. 23.

(20) Zhu, S.; Yao, S.; Wu, F.; Jiang, L.; Wong, K. L.; Zhou, J.; Wang, K. Platinated Porphyrin as a New Organelle and Nucleus Dual-Targeted Photosensitizer for Photodynamic Therapy. *Org. Biomol. Chem.* **2017**, *15*, 5764−5771.

(21) Wang, K. N.; Liu, L. Y.; Qi, G.; Chao, X. J.; Ma, W.; Yu, Z.; Pan, Q.; Mao, Z. W.; Liu, B. Light-Driven Cascade Mitochondria-to-Nucleus Photosensitization in Cancer Cell Ablation. *Adv. Sci.* **2021**, *8*, 2004379.

(22) Tian, X.; Zhu, Y.; Zhang, M.; Luo, L.; Wu, J.; Zhou, H.; Guan, L.; Battaglia, G.; Tian, Y. Localization Matters: A Nuclear Targeting Two-Photon Absorption Iridium Complex in Photodynamic Therapy. *Chem. Commun.* **2017**, *53*, 3303−3306.

(23) Boros, E.; Dyson, P. J.; Gasser, G. Classification of Metal-Based Drugs According to Their Mechanisms of Action. *Chem* **2020**, *6*, 41−60.

(24) Josefsen, L. B.; Boyle, R. Photodynamic Therapy and the Development of Metal-Based Photosensitisers. *Met.-Based Drugs* **2008**, *2008*, No. 276109.

(25) Zhou, Y.; Xia, W.; Liu, C.; Ye, S.; Wang, L.; Liu, R. A DNA and Mitochondria Dual-Targetedphotosensitizer for Two-Photon-Excited-bioimaging and Photodynamic Therapy. *Biomater. Sci.* **2022**, *10*, 1742−1751.

(26) Hurley, L. H. DNA and Its Associated Processes as Targets for Cancer Therapy. *Nat. Rev. Cancer* **2002**, *2*, 188−200.

(27) Sun, J.; Wei, Q.; Zhou, Y.; Wang, J.; Liu, Q.; Xu, H. A Systematic Analysis of FDA-Approved Anticancer Drugs. *BMC Syst. Biol.* **2017**, *11*, No. 87.

(28) Schieber, M.; Chandel, N. S. ROS Function in Redox Signaling. *Curr. Biol.* **2014**, *24*, R453−R462.

(29) Rosenkranz, A. A.; Jans, D. A.; Sobolev, A. S. Targeted Intracellular Delivery of Photosensitizers to enhance photodynamic efficiency. *Immunol. Cell Biol.* **2000**, *78*, 452−464.

(30) Digby, E. M.; Ma, T.; Zipfel, W. R.; Milstein, J. N.; Beharry, A. A. Highly Potent Photoinactivation of Bacteria Using a Water-Soluble, Cell-Permeable, DNA-Binding Photosensitizer. *ACS Infect. Dis.* **2021**, *7*, 3052−3061.

(31) Farhan, N.; Cristofoletti, R.; Basu, S.; Kim, S.; Lingineni, K.; Jiang, S.; Brown, J. D.; Fang, L.; Lesko, L. J.; Schmidt, S. Physiologically-Based Pharmacokinetics Modeling to Investigate Formulation Factors Influencing the Generic Substitution of Dabigatran Etexilate. *CPT:Pharmacometrics Syst. Pharmacol.* **2021**, *10*, 199−210.

(32) Toupin, N. P.; Arora, K.; Shrestha, P.; Peterson, J. A.; Fischer, L. J.; Rajagurubandara, E.; Podgorski, I.; Winter, A. H.; Kodanko, J. J. BODIPY-Caged Photoactivated Inhibitors of Cathepsin B Flip the Light Switch on Cancer Cell Apoptosis. *ACS Chem. Biol.* **2019**, *14*, 2833−2840.

(33) Timney, B. L.; Raveh, B.; Mironska, R.; Trivedi, J. M.; Kim, S. J.; Russel, D.; Wente, S. R.; Sali, A.; Rout, M. P. Simple Rules for Passive Diffusion through the Nuclear Pore Complex. *J. Cell Biol.* **2016**, *215*, 57−76.

(34) Colwell, L. J.; Brenner, M. P.; Ribbeck, K. Charge as a Selection Criterion for Translocation through the Nuclear Pore Complex. *PLoS Comput. Biol.* **2010**, *6*, No. e1000747.

(35) Krumova, K.; Cosa, G. Bodipy Dyes with Tunable Redox Potentials and Functional Groups for Further Tethering: Preparation, Electrochemical, and Spectroscopic Characterization. *J. Am. Chem. Soc.* **2010**, *132*, 17560−17569.

(36) Peterson, J. A.; Fischer, L. J.; Gehrmann, E. J.; Shrestha, P.; Yuan, D.; Wijesooriya, C. S.; Smith, E. A.; Winter, A. H. Direct Photorelease of Alcohols from Boron-Alkylated BODIPY Photocages. *J. Org. Chem.* **2020**, *85*, 5712−5717.

(37) Bennion, B. J.; Be, N. A.; McNerney, M. W.; Lao, V.; Carlson, E. M.; Valdez, C. A.; Malfatti, M. A.; Enright, H. A.; Nguyen, T. H.; Lightstone, F. C.; Carpenter, T. S. Predicting a Drug's Membrane Permeability: A Computational Model Validated with in Vitro Permeability Assay Data. *J. Phys. Chem. B* **2017**, *121*, 5228−5237.

https://doi.org/10.1021/acs.jmedchem.2c01504
J. Med. Chem. 2022, 65, 16679−16694

(38) Hard, T.; Fan, P.; Kearns, D. R. A Fluorescence Study of the Binding of Hoechst 33258 and DAPI to Halogenated DNAs. *Photochem. Photobiol.* **1990**, *51*, 77−86.
(39) Biyiklioglu, Z.; Barut, B.; Özel, A. Synthesis, DNA/BSA Binding and DNA Photocleavage Properties of Water Soluble BODIPY Dyes. *Dyes Pigm.* **2018**, *148*, 417−428.
(40) Keleş, T.; Barut, B.; Yıldırım, S.; Yalçın, C. Ö.; Biyiklioglu, Z. Synthesis of Water-Soluble BODIPY Dyes and Investigation of Their DNA Interaction Properties and Cytotoxicity/Phototoxicity. *Appl. Organomet. Chem.* **2021**, *35*, No. e6410.
(41) Zhao, C.; Zhang, Y.; Wang, X.; Cao, J. Development of BODIPY-Based Fluorescent DNA Intercalating Probes. *J. Photochem. Photobiol., A* **2013**, *264*, 41−47.
(42) Ligasová, A.; Koberna, K. Quantification of Fixed Adherent Cells Using a Strong Enhancer of the Fluorescence of DNA Dyes. *Sci. Rep.* **2019**, *9*, No. 8701.
(43) Prole, D. L.; Chinnery, P. F.; Jones, N. S. Visualizing, Quantifying, and Manipulating Mitochondrial DNA in Vivo. *J. Biol. Chem.* **2020**, *295*, 17588−17601.
(44) Ghosh, A. K.; Brindisi, M. Organic Carbamates in Drug Design and Medicinal Chemistry. *J. Med. Chem.* **2015**, *58*, 2895−2940.
(45) Reiniers, M. J.; van Golen, R. F.; Bonnet, S.; Broekgaarden, M.; van Gulik, T. M.; Egmond, M. R.; Heger, M. Preparation and Practical Applications of 2′,7′- Dichlorodihydrofluorescein in Redox Assays. *Anal. Chem.* **2017**, *89*, 3853−3857.
(46) Zhao, X.; Liu, J.; Fan, J.; Chao, H.; Peng, X. Recent Progress in Photosensitizers for Overcoming the Challenges of Photodynamic Therapy: From Molecular Design to Application. *Chem. Soc. Rev.* **2021**, *50*, 4185−4219.
(47) Ouédraogo, G. D.; Redmond, R. W. Secondary Reactive Oxygen Species Extend the Range of Photosensitization Effects in Cells: DNA Damage Produced Via Initial Membrane Photosensitization. *Photochem. Photobiol.* **2003**, *77*, 192.
(48) Douillard, S.; Rozec, B.; Bigot, E.; Aillet, L.; Patrice, T. Secondary Reactive Oxygen Species Production after PDT during Pulmonary Tumor Growth in Sera of Nude Mice. *Photodiagn. Photodyn. Ther.* **2013**, *10*, 62−71.
(49) Collin, F. Chemical Basis of Reactive Oxygen Species Reactivity and Involvement in Neurodegenerative Diseases. *Int. J. Mol. Sci.* **2019**, *20*, 2407.
(50) Kroemer, Y.How to Interpret DNA Gel Electrophoresis Results. https://www.goldbio.com/articles/article/Interpreting-Gel-Electrophoresis-Results.
(51) Collins, P. L.; Purman, C.; Porter, S. I.; Nganga, V.; Saini, A.; Hayer, K. E.; Gurewitz, G. L.; Sleckman, B. P.; Bednarski, J. J.; Bassing, C. H.; Oltz, E. M. DNA Double-Strand Breaks Induce H2Ax Phosphorylation Domains in a Contact-Dependent Manner. *Nat. Commun.* **2020**, *11*, No. 3158.
(52) Kuo, L. J.; Yang, L. X. γ-H2AX- A Novel Biomarker for DNA Double-Strand Breaks. *In Vivo* **2008**, *22*, 305−309.
(53) Kim, M. M.; Darafsheh, A. Light Sources and Dosimetry Techniques for Photodynamic Therapy. *Photochem. Photobiol.* **2020**, *96*, 280−294.
(54) Huang, Z.; Xu, H.; Meyers, A. D.; Musani, A. I.; Wang, L.; Tagg, R.; Barqawi, A. B.; Chen, Y. K. Photodynamic Therapy for Treatment of Solid Tumors - Potential and Technical Challenges. *Technol. Cancer Res. Treat.* **2008**, *7*, 309−320.
(55) Cui, S.; Yin, D.; Chen, Y.; Di, Y.; Chen, H.; Ma, Y.; Achilefu, S.; Gu, Y. In Vivo Targeted Deep-Tissue Photodynamic Therapy Based on near-Infrared Light Triggered Upconversion Nanoconstruct. *ACS Nano* **2013**, *7*, 676−688.
(56) Brüningk, S. C.; Rivens, I.; Box, C.; Oelfke, U.; ter Haar, G. 3D Tumour Spheroids for the Prediction of the Effects of Radiation and Hyperthermia Treatments. *Sci. Rep.* **2020**, *10*, No. 1653.
(57) Zanoni, M.; Piccinini, F.; Arienti, C.; Zamagni, A.; Santi, S.; Polico, R.; Bevilacqua, A.; Tesei, A. 3D Tumor Spheroid Models for in Vitro Therapeutic Screening: A Systematic Approach to Enhance the Biological Relevance of Data Obtained. *Sci. Rep.* **2016**, *6*, No. 19103.
(58) Perillo, B.; Di Donato, M.; Pezone, A.; Di Zazzo, E.; Giovannelli, P.; Galasso, G.; Castoria, G.; Migliaccio, A. ROS in Cancer Therapy: The Bright Side of the Moon. *Exp. Mol. Med.* **2020**, *52*, 192−203.
(59) Slanina, T.; Shrestha, P.; Palao, E.; Kand, D.; Peterson, J. A.; Dutton, A. S.; Rubinstein, N.; Weinstain, R.; Winter, A. H.; Klán, P. In Search of the Perfect Photocage: Structure-Reactivity Relationships in Meso-Methyl BODIPY Photoremovable Protecting Groups. *J. Am. Chem. Soc.* **2017**, *139*, 15168−15175.

https://doi.org/10.1021/acs.jmedchem.2c01504
J. Med. Chem. 2022, 65, 16679−16694